[redacted]

ORNL
MASTER COPY

AEC RESEARCH AND DEVELOPMENT REPORT

ORNL-2660
C-86 - Nuclear Rocket
and Ram-Jet Engines

THIS DOCUMENT WAS PRIMARILY DECLASSIFIED
AND IS EXEMPT FROM DOE 1979 REVIEW
PER DOE LETTER, 10-15-79, R. T. BRAY, DOE
P. S. BAKER, ORNL/CO 04 / 3/5/80
INITIALS DATE

DOE 1979 REVIEW OF
DECLASSIFIED REPORTS

This Document is Properly Declassified.

Reviewed by P. S. Baker OCT 1 8 1979
ORNL Classification Officer PSB

A PRELIMINARY EXPERIMENTAL STUDY OF VORTEX TUBES FOR GAS-PHASE FISSION HEATING

J. L. Kerrebrock
J. J. Keyes, Jr.

DECLASSIFIED By Authority Of:
AEC 8-19-60
JMH
For: R. T. Bray, Supervisor
Laboratory Records Dept.
ORNL

OAK RIDGE NATIONAL LABORATORY
operated by
UNION CARBIDE CORPORATION
for the
U.S. ATOMIC ENERGY COMMISSION

[redacted]

[redacted]

LEGAL NOTICE

This report was prepared as an account of Government sponsored work. Neither the United States, nor the Commission, nor any person acting on behalf of the Commission:

A. Makes any warranty or representation, express or implied, with respect to the accuracy, completeness, or usefulness of the information contained in this report, or that the use of any information, apparatus, method, or process disclosed in this report may not infringe privately owned rights; or

B. Assumes any liabilities with respect to the use of, or for damages resulting from the use of any information, apparatus, method, or process disclosed in this report.

As used in the above, "person acting on behalf of the Commission" includes any employee or contractor of the Commission to the extent that such employee or contractor prepares, handles or distributes, or provides access to, any information pursuant to his employment or contract with the Commission.

[redacted]

ORNL-2660

C-86 - NUCLEAR ROCKET ENGINES

This document consists of 54 pages.
Copy 33 of 148 copies. Series A.

Contract No. W-7405-eng-26

Reactor Projects Division

A PRELIMINARY EXPERIMENTAL STUDY OF VORTEX TUBES FOR GAS-PHASE FISSION HEATING

J. L. Kerrebrock

J. J. Keyes, Jr.

Date Issued

FEB 6 1959

OAK RIDGE NATIONAL LABORATORY
Operated by
UNION CARBIDE CORPORATION
for the
U. S. ATOMIC ENERGY COMMISSION

[redacted]

[redacted]

[redacted]

[redacted]

TABLE OF CONTENTS

	Page
SUMMARY	1
INTRODUCTION	2
APPARATUS AND INSTRUMENTATION	6
PRESENTATION AND ANALYSIS OF RESULTS	13
Viscous Effects	13
Influence of Exit Nozzle on Vortex Structure	24
Preliminary Separation Experiments	29
CONCLUSIONS	45
REFERENCES	46

LIST OF FIGURES

Fig. No.		Page
1	Schematic Diagram of a Vortex Tube Applied to Rocket Propulsion	3
2	Sketch of Experimental Vortex Tube	7
3	Plastic Test Block - Vortex Tube No. 1	8
4	Vortex Tube Holder	10
5	Over-all Flow and Instrumentation Diagram	12
6	Typical Correlation of Measured Pressure Distribution with Eq. 6	16
7	Typical Correlation of Ratio of Pressure to Wall Pressure with Eq. 6	17
8	Variation of ϵ in $v \propto r^{+\epsilon}$ with Mass Flow Rate per Unit of Tube Length, and Tube Pressure, for Tube No. 2	19
9	Variation of ϵ in $v \propto r^{+\epsilon}$ with Mass Flow Rate per Unit of Tube Length, and Tube Pressure, for Tube No. 1	20
10	Variation of Ratio of Vortex Tangential Mach Number and Jet Exit Mach Number with Mass Flow Rate per Unit of Tube Length, and Tube Pressure, for Tube No. 2	22
11	Variation of Ratio of Vortex Tangential Mach Number and Jet Exit Mach Number with Mass Flow Rate per Unit of Tube Length, and Tube Pressure, for Tube No. 1	23
12	Variation of Tangential Velocity with Radius Within Region Influenced by Exit Nozzle Outflow, for Various Effective Viscosities, K	26
13	Dependence of I(0,K) on the Effective Viscosity, K	27
14	Pressure Distributions and Correlation Parameters for two Different Exit Nozzle Configurations	28
15	Photographs Taken Axially Through Vortex Tube Operating with He and Br_2, Showing at the Left a Large Ring of Condensed Br_2, and at the Right only the Condensed Br_2	31

LIST OF FIGURES (Continued)

Fig. No.		Page
16	Pressure Distributions Corresponding to the Photographs of Fig. 15	33
17	Mach Number Distributions Corresponding to the Photographs of Fig. 15, with Values of Mach Number Required for Separation, M_m	34
18	Sample Probe Detail	37
19	Effect of Sampling Probe on Pressure Distribution	38
20	Gas Analysis Apparatus	40
21	Measured Mole Fraction of C_8F_{16} in Helium, for two Modes of Introduction of the Fluorocarbon	41
22	Pressure Profile Corresponding to Fig. 21	43
23	Mach Number Profile Corresponding to Fig. 21	44

A PRELIMINARY EXPERIMENTAL STUDY OF VORTEX TUBES FOR GAS-PHASE FISSION HEATING

J. L. Kerrebrock J. J. Keyes, Jr.

SUMMARY

An experimental study of a simple jet-driven vortex tube has indicated that the viscous retardation of the vortex motion is so severe as to prevent the formation of vortices of sufficient strength for vortex-cavity reactor applications. The large viscous effects are most likely due to the existence of turbulent flow in the tube; hence a second experimental study, aimed at production of laminar vortices, has been initiated.

Even though the viscous effects in the vortices are very strong, the variation of tangential velocity with radius is near that for an inviscid vortex, with the velocity being proportional to the radius to a power which varies between -0.4 and -0.8.

A simple model representing the influence of the outflow through the central exit nozzle on the vortex core structure is proposed. Satisfactory agreement with the measured pressure distributions near the vortex center has been found.

Although the tangential Mach numbers generated in the present apparatus are too low to permit separation of gases under the conditions required in vortex-cavity reactors, preliminary separations of helium from both bromine and a heavy fluorocarbon (C_8F_{16}) have been obtained. The heavy gas concentration peaks were very near the center of the vortex tube, at radial positions which are in reasonably good agreement with the predictions of the analysis of Ref. 1.

INTRODUCTION

The capabilities of vortex tubes for the production of very hot gases by fission heating have been explored analytically.[1] A schematic drawing of such a vortex tube, applied to rocket propulsion, is shown in Fig. 1. A low molecular weight gas is introduced to the tube tangentially, so that a vortex motion is produced. The light gas flows spirally inward, diffusing through a cloud of high-molecular-weight fissionable gas. The heavy gas is held against the radial mass flow by the centrifugal force field produced by the vortex. After passing through the cloud of fissionable gas and absorbing the heat generated in it by fission, the light gas flows down the center of the tube and out through a nozzle at one end.

In the analytical study of this device, three important assumptions were made: the flow was assumed to be laminar, inviscid, and two-dimensional, with complete uniformity along the axis of the tube. The analysis indicated that under these conditions the vortex tube should be capable of producing high gas temperature ratios at mass flow rates of the order of 0.01 pounds per second per foot of tube length, as limited by the diffusion of the light gas through the heavy gas. The inlet tangential Mach numbers required were about unity. That this mass flow rate is rather low may be seen by comparison with "Hilsch Tube" experiments,[2] in which the mass flow is about ten times as large.

It was concluded in Ref. 1 that essentially inviscid vortices can be generated at these low mass flow rates if the flow is laminar. However, if the flow is turbulent, it becomes difficult to estimate the viscous effects on the vortex strength.

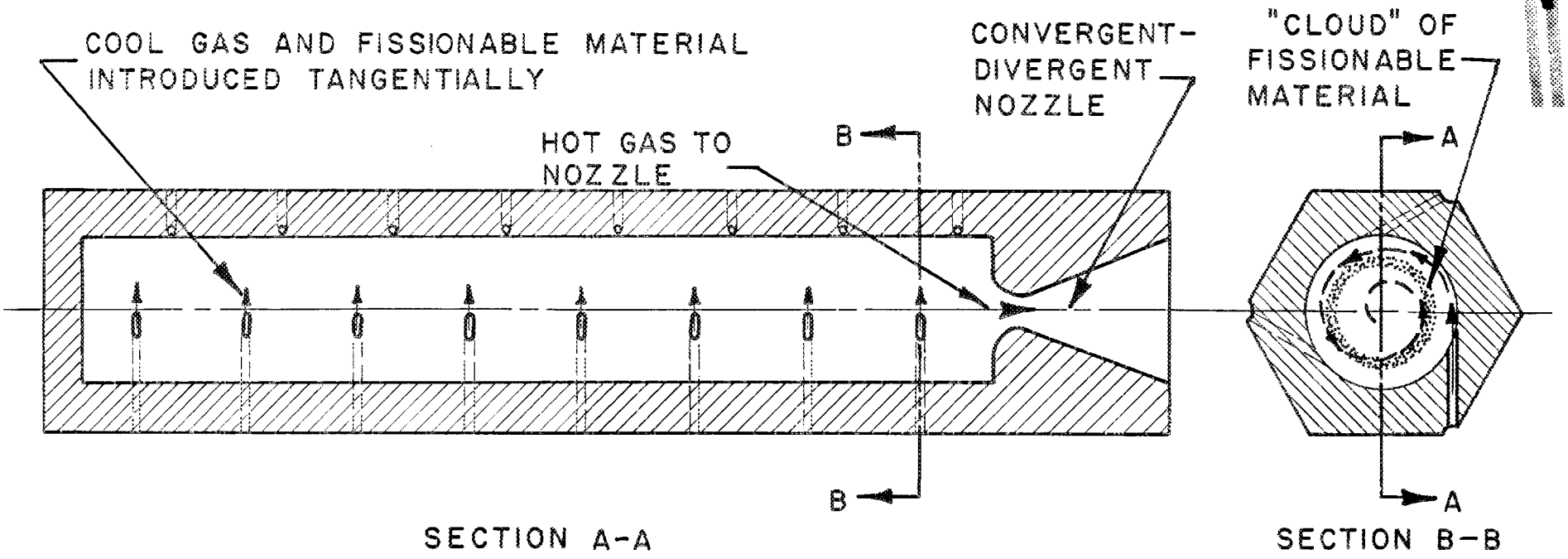

SPECIALIZATION OF THE VORTEX TUBE FOR ROCKET PROPULSION.

A UNIT VORTEX CELL WITH INTEGRAL NOZZLE

FIGURE 1

ORNL-LR-Dwg.-24782

In view of these facts, the experimental study of vortex-separation tubes has been divided into two distinct experiments. The purpose of the first experiment was principally to determine the magnitude of viscous effects on the vortex strength. In addition, an estimate of the influence of the outflow through the nozzle on the vortex structure has been obtained. Preliminary separation experiments have been carried out, but under flow conditions far removed from the design point. While this experiment cannot be regarded as a successful demonstration of separation from the standpoint of application to vortex reactors, it is useful as a reference point for the analysis of Ref. 1. The results of these first experiments are given in this report.

Since it was expected, and later confirmed experimentally, that the viscous effects for turbulent flow would be so strong as to prevent the formation of vortices of adequate strength, a second experimental study aimed at production of laminar vortices has also been initiated. The method to be explored consists of bleeding a portion of the inlet nozzle mass flow from the vortex tube through a uniformly porous tube wall. An analytical study of this idea[3] indicated that it should be possible to stabilize the shear layer on the tube wall for reasonable bleed mass flows. The results of this experiment will be reported in a second document.

A detailed description of the apparatus and instrumentation for the first experiment is given in the body of the report; however, some key design criteria will be mentioned here. The design of the experiment was based on three similarity parameters: the nozzle inlet Mach number, the Reynolds number based on the tube diameter and tangential velocity, and the

ratio of radial mass flow rate to dynamic viscosity. The design and operating conditions of the tube were so chosen that each of these parameters would be equal to that for a typical high temperature vortex tube as described in Ref. 1, Table I. The necessity for equality of the first two parameters is obvious. The last parameter was found, in Ref. 1, to govern the magnitude of viscous effects on the vortex strength. It is really a Reynolds number based on the radial flow velocity and tube radius.

An essential feature of the vortex tubes being considered here is that the fluid is introduced nearly uniformly over the peripheral surface of the tube so that a uniform radial flow is established. With the low mass flow rates and high tangential velocities required by the diffusion process, the inlet nozzle area is necessarily very small. Thus, the nozzle configuration which has been chosen is a series of very small discrete jets, evenly spaced around the periphery of the tube.

The presentation of results is based on correlation of the data with predictions from simple analytical models, rather than the presentation of large amounts of original data. Thus, the results will consist largely of the values which the parameters of the analytical models must have in order to best correlate the data; however, some examples of the agreement of the experimental data with the predictions of the models are also given.

APPARATUS AND INSTRUMENTATION

The geometry selected for the initial experiments is a 1-ft section of vortex tube of 2-in. inside diameter, bored in a 4-in. Lucite block, as sketched in Fig. 2. Twelve brass feed nozzles are located in the wall of the block so as to form a broken spiral of entrance jets spaced 1-in. axially with 90-deg rotation between adjacent nozzles and continuing the length of the block. The inside surfaces of the nozzles are honed flush with the inside diameter of the tube, as shown in the detail. Two such vortex tubes, differing only in size and location of the feed nozzles, have been run. These are compared below:

Vortex Tube No.	Inlet Nozzle Diameter	Radial Position of Nozzle, r'
1	0.0135 in.	0.92
2	0.0100 in.	0.84

Note that for a given supply pressure, tube No. 1 will pass about 80 per cent more mass flow than tube No. 2.

The feed nozzles are supplied with gas from four headers drilled in the plastic block so that each one feeds three nozzles in line. Fig. 3 is a photograph of tube No. 1 showing the arrangement of feed headers and nozzles. Note the use of "O"-ring seals between the tube proper and header channels (top of photograph) and the supply plate. The exit plate is likewise sealed. Thus, the vortex tube can be readily removed and the end plates interchanged. The three tubes seen projecting outward are wall pressure taps. Gas exhausts at one end through an adjustable annular orifice directly to the atmosphere, as shown in Fig. 2. Other exit configurations which have been

ORNL-LR-DWG 32566

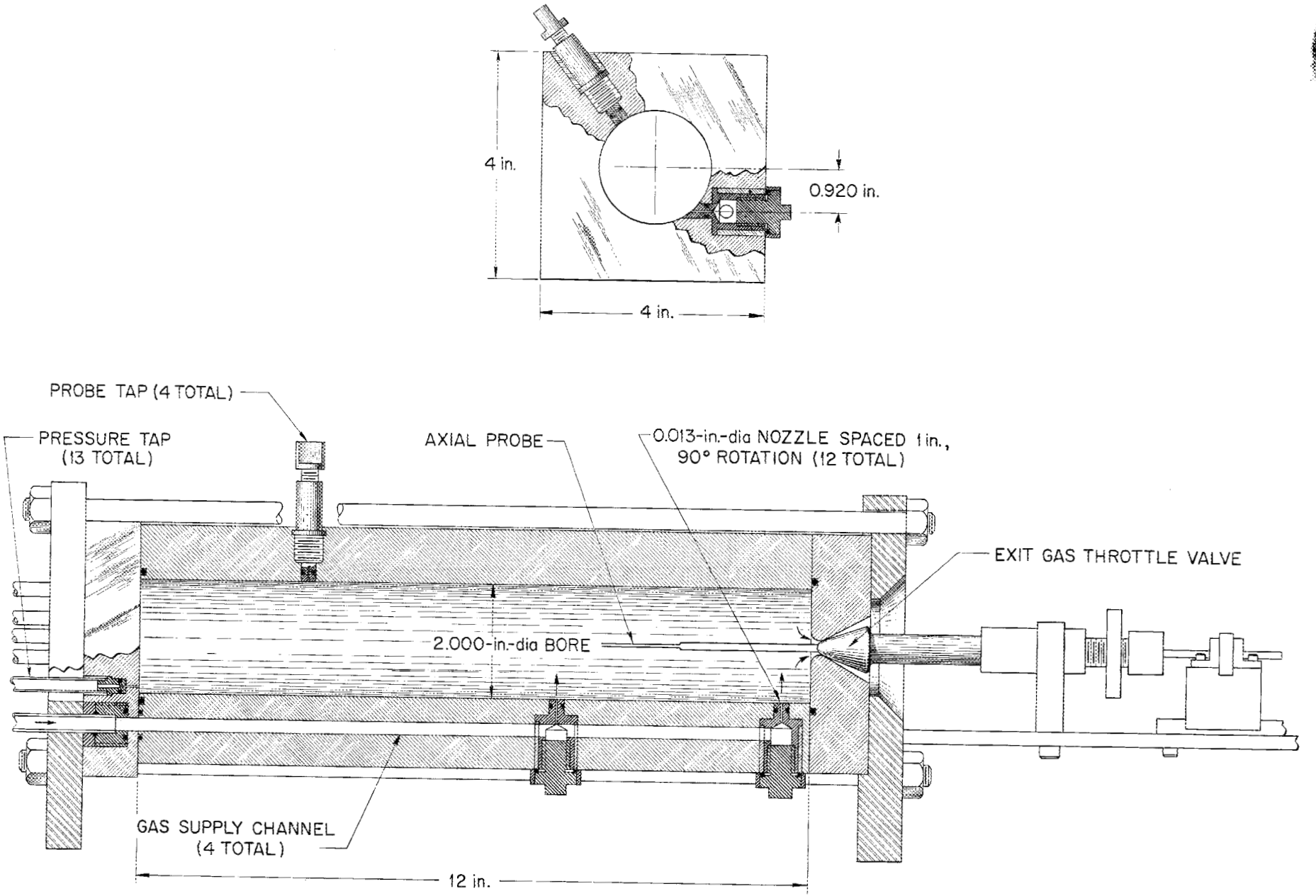

Fig. 2. Sketch of Experimental Vortex Tube.

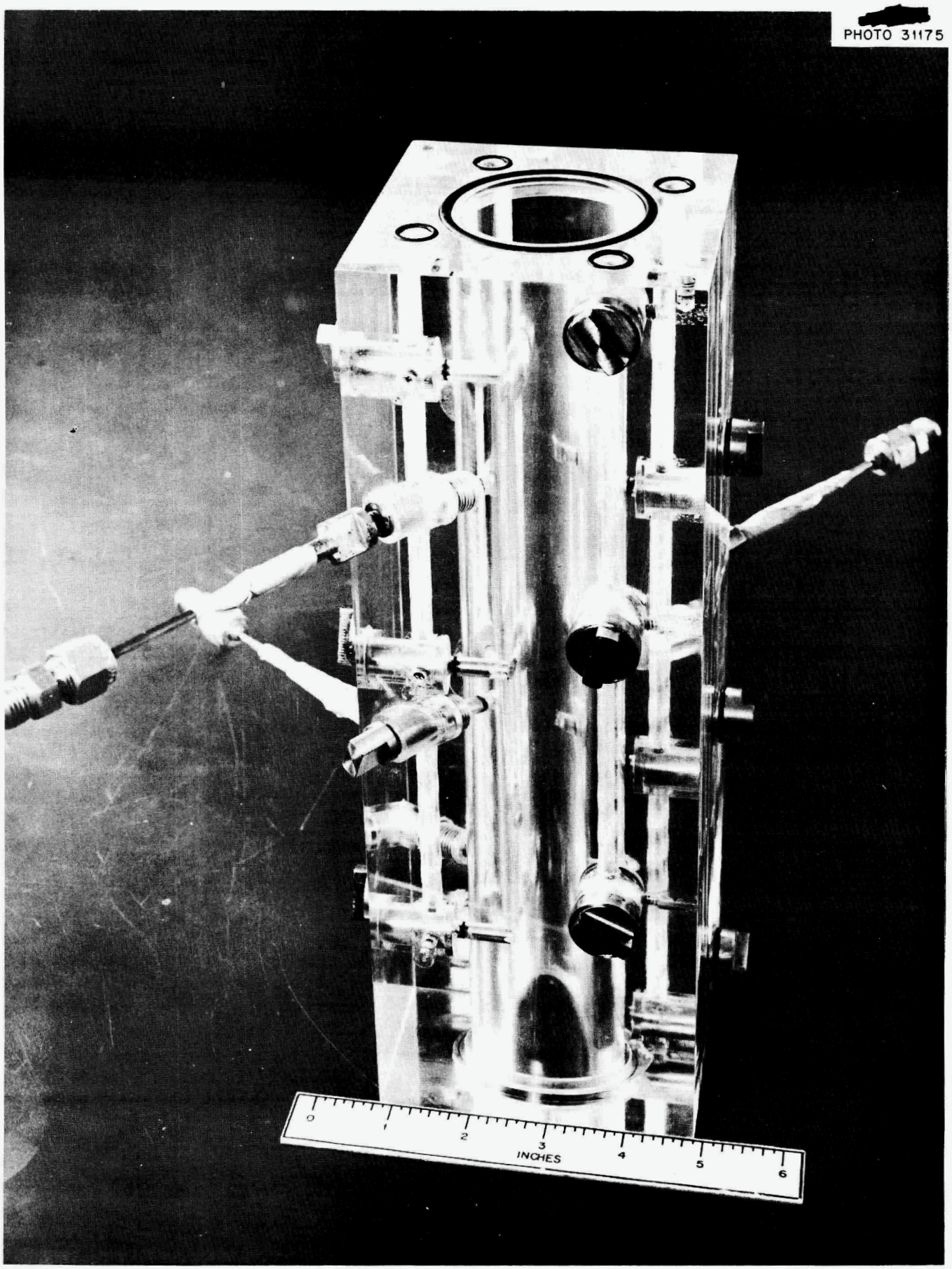

Fig. 3. Plastic Test Block – Vortex Tube No. 1.

explored are discussed later.

In order to measure the radial static pressure distribution, a number of pressure taps are located in the feed plate as seen at the left of Fig. 2. Fig. 4 is a photograph of the frame and end-plates with the block removed, showing the adjustable exit orifice and axial probe at the left, and the feed plate at the right. The layout of the thirteen pressure taps on a close spiral starting at the center is clearly shown. The radial position of the taps is tabulated below:

Tap No.	Radial Position r'	Tap No.	Radial Position r'
1	0.000	8	0.570
2	0.093	9	0.703
3	0.203	10	0.820
4	0.320	11	0.875
5	0.375	12	0.938
6	0.438	13	1.000
7	0.493		

Taps 2 and 3 are not visible in the photograph.

In addition to the end pressure taps, several probe taps entering radially through the wall are included (as shown in Figs. 2 and 3). These are used to measure static wall pressure and can accommodate the sampling probe used in the separation experiments. Also included is an axial pressure and sampling probe which can be run into the tube by a rack and pinion drive.

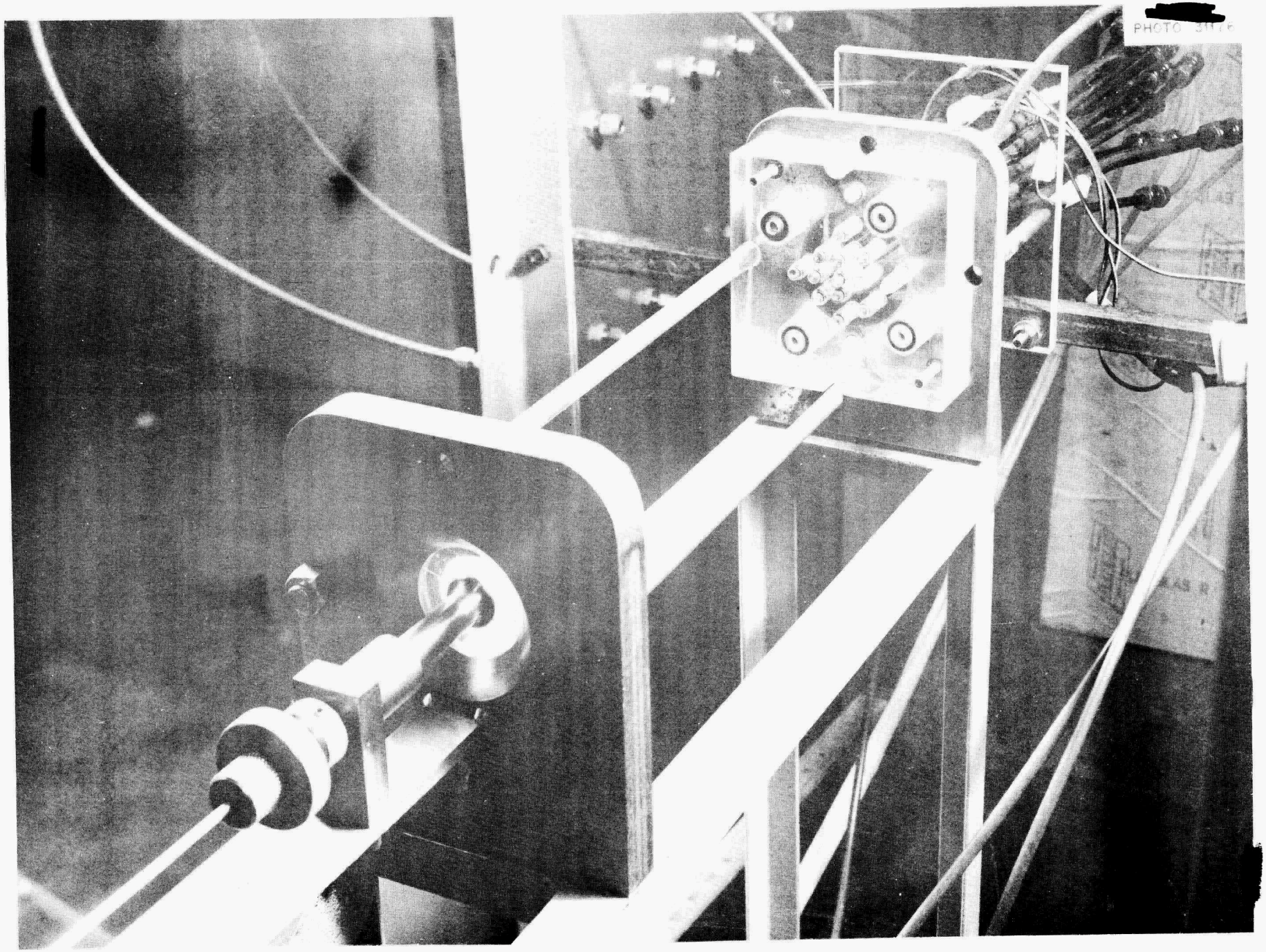

Fig. 4. Vortex Tube Holder.

Fig. 5 is the over-all flow and instrumentation diagram. Helium or nitrogen gas is supplied from cylinder banks through pressure regulators and appropriate metering devices to each of the four supply headers at pressures up to 600 psig, as read by Bourdon-type test gauges upstream of the feed-plate entrance. Valves are provided for controlling the individual header flows if necessary. The pressure in the vortex tube is regulated by the exit valve up to a maximum of 150 psig. All pressure measuring taps are connected to "quick-connect" plug-in couplings, panel mounted, with provision for manual connection to any of four gauges to read absolute or differential pressure. In addition, a manometer bank is connected to read ten pressure differentials simultaneously as indicated in the diagram. The absolute pressure measurements are good to ± 0.2 per cent of full scale (150 psi), and the differential measurements to 2 per cent or better.

Provision has been made for adding a trace-gas component by saturation of a portion of the supply gas in a bubbler tank. The gas thus saturated can be introduced through the tangential nozzles, or through the wall or end pressure taps. Thermocouples are provided to measure inlet gas temperature and tank temperature.

[redacted]

ORNL-LR-DWG 32289

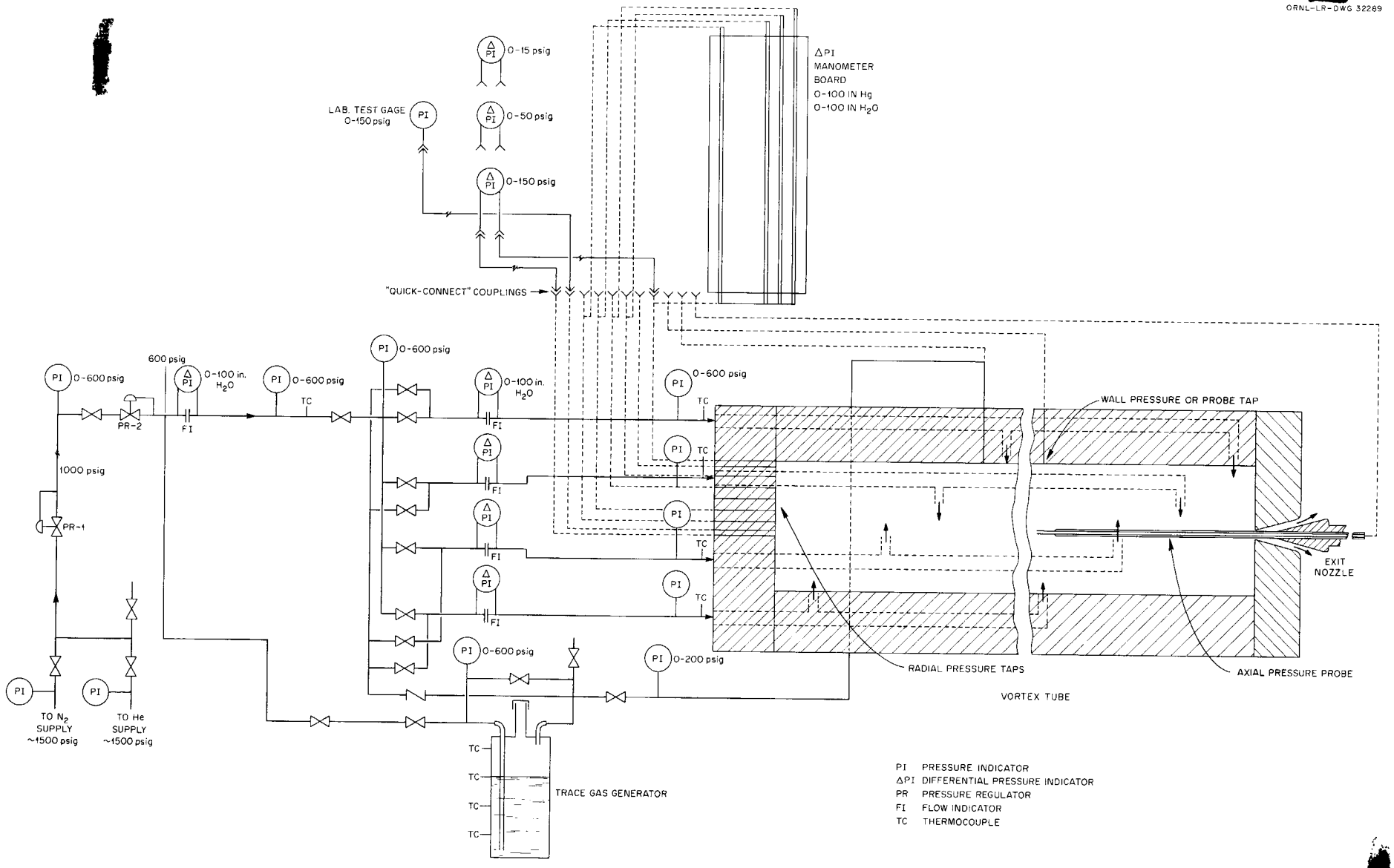

Fig. 5. Over-all Flow and Instrumentation Diagram.

[redacted]

PRESENTATION AND ANALYSIS OF RESULTS

Viscous Effects

For laminar flow with negligible axial velocity, the tangential momentum equation may be written as

$$\frac{dv}{dr} + \frac{v}{r} = \frac{\mu}{\rho u} \left\{ \frac{d^2v}{dr^2} + \frac{1}{r} \frac{dv}{dr} - \frac{v}{r^2} \right\}$$

where v and u are the tangential and radial velocities, respectively, ρ is the density, and r is the radius. For the present purposes, it is convenient to rewrite the equation in terms of the tangential velocity divided by its value near the wall of the tube, and the radius divided by the tube radius. If we denote these quantities by primes, we find

$$\frac{dv'}{dr'} + \frac{v'}{r'} = \left(\frac{\mu}{\rho ur}\right) r' \left\{ \frac{d^2v'}{dr'^2} + \frac{1}{r'} \frac{dv'}{dr'} - \frac{v'}{r'^2} \right\} \tag{1}$$

If μ is interpreted as the sum of the actual viscosity and the apparent viscosity due to turbulence, this equation may also be applied to turbulent flow. If the effective μ is also assumed constant, then since ρur is constant, we may write the equation as

$$r'^2 \frac{d^2v'}{dr'^2} + r'\left(1 + \frac{1}{K}\right) \frac{dv'}{dr'} - \left(1 - \frac{1}{K}\right) v' = 0 \tag{2}$$

where $K = \mu/\rho ur$.

The solution of Eq. 2 is

$$v' = A_1(r')^{-1} + A_2(r')^{-\frac{1-K}{K}}$$

For $K \to 0$, the flow must approach a free vortex flow, for which v' is

proportional to r'^{-1}; hence for $K \to 0$, the second term, which is proportional to r' to a large negative power, must be negligible. For any given small K, this second term is most important for small r', so as K increases from 0, we expect a deviation from the r^{-1} behavior first at small r'. As K increases, the second term should become significant over a larger range of r', until for K of order unity, the two terms are of about equal importance over the full range of r'. In particular, for $K = 1/2$, both terms are proportional to r^{-1}.

Since the power of r' in the second term varies from 0 to +1 as K increases from 0 to $+\infty$, it is not inconsistent with this exact solution of Eq. 2 to assume that v' is given by

$$v' = Cr'^{\epsilon} \tag{3}$$

where $-\epsilon$ is between unity and zero. If K is very small, this single term must be regarded as a sum of the two terms in the previous equation; however, for K between $+\infty$ and 1/2, the second term alone gives $-\epsilon$ from -1 to 1. Thus, for the present, we make the identification

$$-\epsilon = \frac{1 - K}{K} \quad ; \quad K = \frac{1}{1 - \epsilon} \tag{4}$$

The reasonableness of this choice will be indicated later by comparison with the data.

The radial pressure gradient is given in terms of the tangential velocity by

$$\frac{dp}{dr} = \rho \frac{v^2}{r} ,$$

or in terms of the dimensionless variables, by

$$\frac{1}{p'} \frac{dp'}{dr'} = \gamma M_p^2 \frac{v'^2}{r'T'} \tag{5}$$

where M_p is the tangential Mach number of the vortex at $r' = 1$. The temperature variation is closely given by

$$T' = (p')^{\frac{\gamma - 1}{\gamma}}$$

Using this relation and Eq. 3, in Eq. 5, and integrating, we find

$$1 - (p')^{\frac{\gamma - 1}{\gamma}} = \frac{(\gamma - 1)M_p^2}{-2\epsilon} \left[\frac{1}{(r')^{-2\epsilon}} - 1 \right] \tag{6}$$

For properly chosen values of ϵ and M_p, Eq. 6 fits the experimental pressure distribution in the vortex tube quite accurately. An example of such a correlation is shown in Fig. 6. This run was made with the tube No. 2, with the annular exit orifice 0.28 in. in outside diameter, nitrogen as the working fluid, and inlet manifold and tube wall pressures of 545 and 63.8 psia, respectively. The ideal jet exit Mach number for this pressure ratio is 2.06, while the actual tangential Mach number of the vortex was 0.0763. The exponent, ϵ, was -0.695, and this gives K = 0.590.

The comparison shown in Fig. 6 is a very sensitive indication of the precision with which Eq. 6 fits the data, since the quantity $1 - (p')^{\frac{\gamma - 1}{\gamma}}$ varies by two orders of magnitude, and there is an inflection in the curve. The actual pressure, p', does not deviate significantly from the computed curve, except near the center of the tube where the influence of the exit nozzle is felt. This is shown in Fig. 7.

Although the fit is very good, there is still the possibility that a combination of the two terms of the solution of Eq. 2 would give as good a

[redacted]

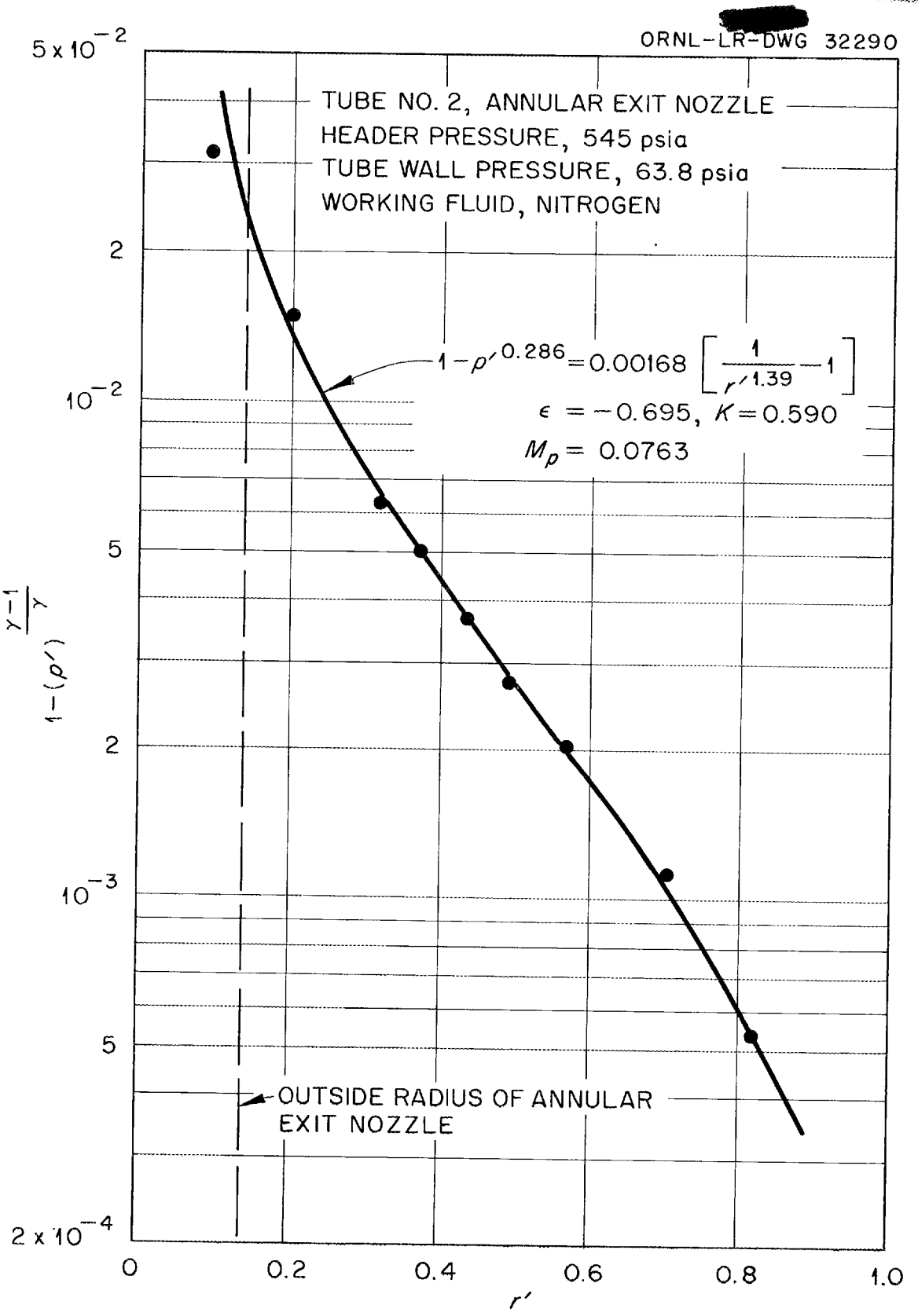

Fig. 6. Typical Correlation of Measured Pressure Distribution with Eq. (6).

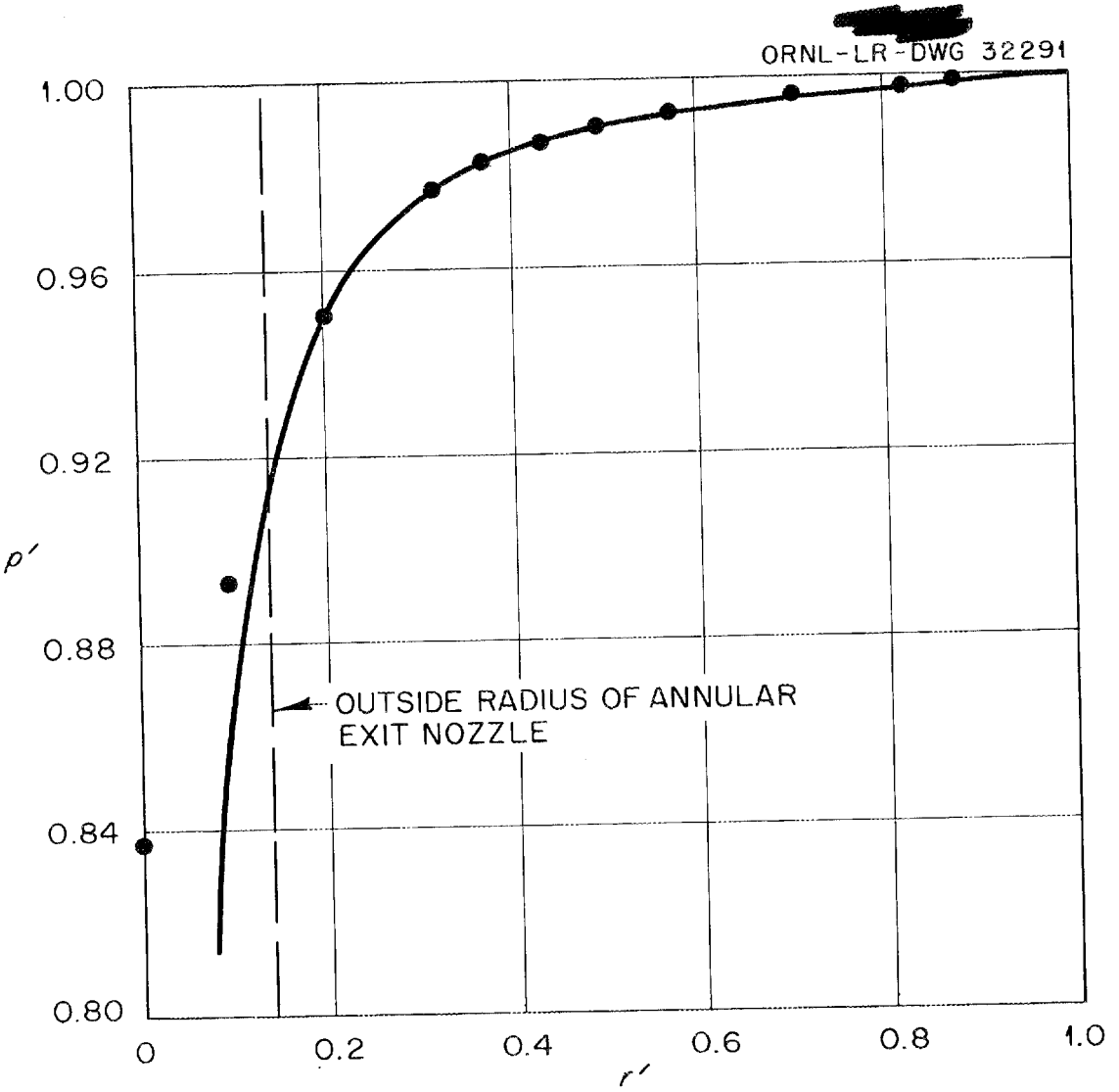

Fig. 7. Typical Correlation of Ratio of Pressure to Wall Pressure with Eq. (6)

fit for some value of K much less than 0.590. However, it will be shown later that the analysis of the influence of the nozzle outflow on the vortex structure indicates that a K of 0.590 is of about the right magnitude to explain the measured pressure distribution near the vortex center.

In view of the excellent fit obtained with Eq. 6, the bulk of the pressure distribution data has been reduced by computing single values of M_p and ϵ for each experiment. The quantities which could be varied for a given run were the header pressure and the tube pressure. Since the inlet nozzles were choked (sonic) at nearly all operating conditions, the mass flow rate per unit of tube length, $\mathcal{M}_1$ was simply proportional to the header pressure.

The variation of ϵ with mass flow rate and tube pressure is shown in Fig. 8 for tube No. 2 and in Fig. 9 for tube No. 1. These values were computed by fitting Eq. 6 to the pressure measurements at two points on the tube radius. Thus the scatter may be due to uncertainties in measurements at these two particular points. The uncertainty could probably be reduced by a least-squares fit of Eq. 6 to the pressure distribution for each run, but the amount of labor involved in such a fitting process appeared prohibitive.

In spite of the scatter of the values of ϵ, two points are clear. First, the values of ϵ are very much closer to the value (-1) for a free vortex than to the value (+1) for a solid body rotation. The values of K, computed from Eq. 4, range from 0.7 to 0.55 as $-\epsilon$ varies from 0.4 to 0.8. Second, the values of $-\epsilon$ do increase with increasing $\mathcal{M}_1$ (at least up to about $\mathcal{M}_1 = 0.01$ lb/sec·ft) as would be expected if the effective viscosity were nearly constant. There is also some effect of tube pressure, which may

[redacted]

[redacted]

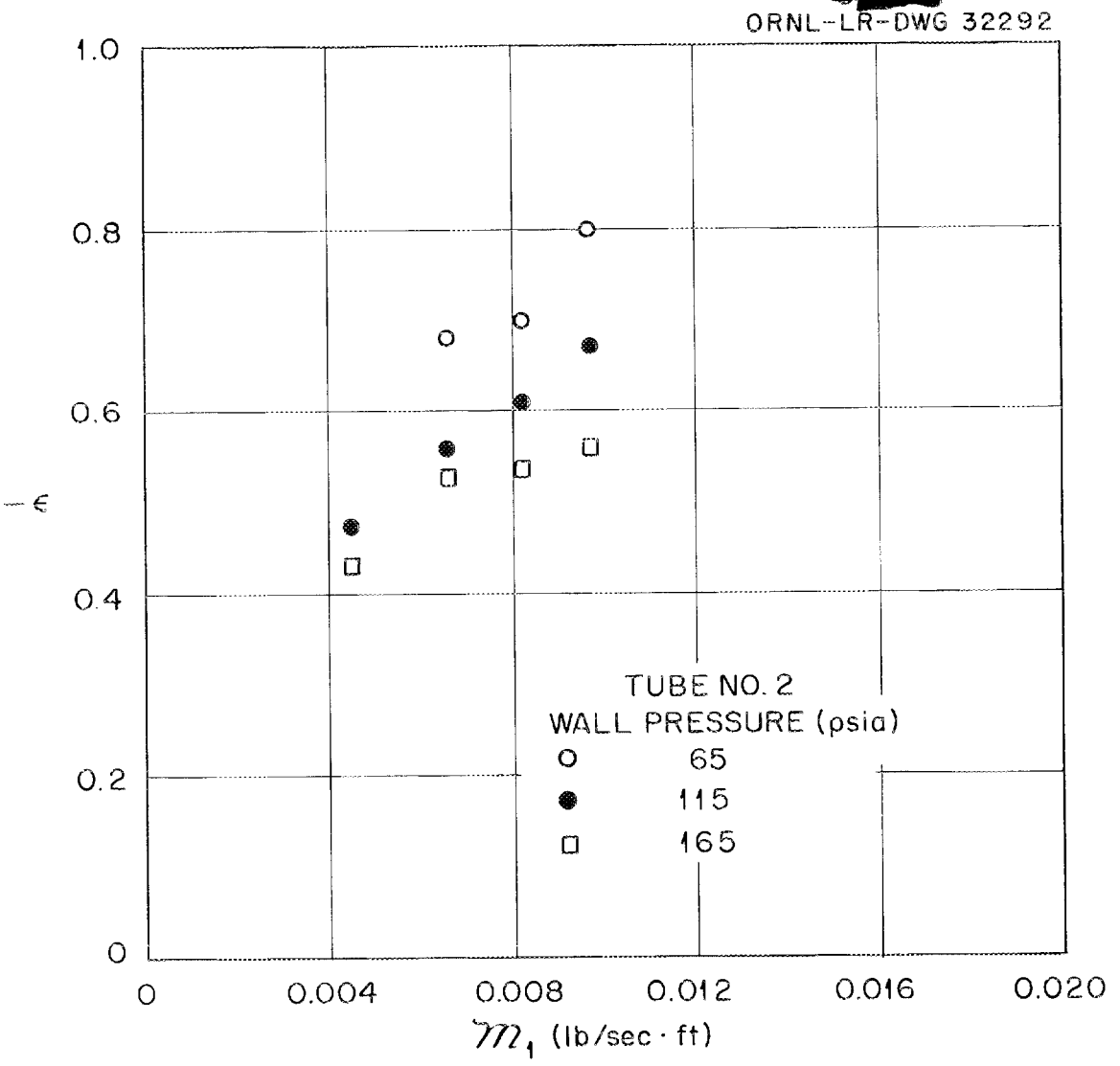

Fig. 8. Variation of ϵ in $\nu \propto r^{+\epsilon}$ with Mass Flow Rate per Unit of Tube Length, and Tube Pressure, for Tube No. 2.

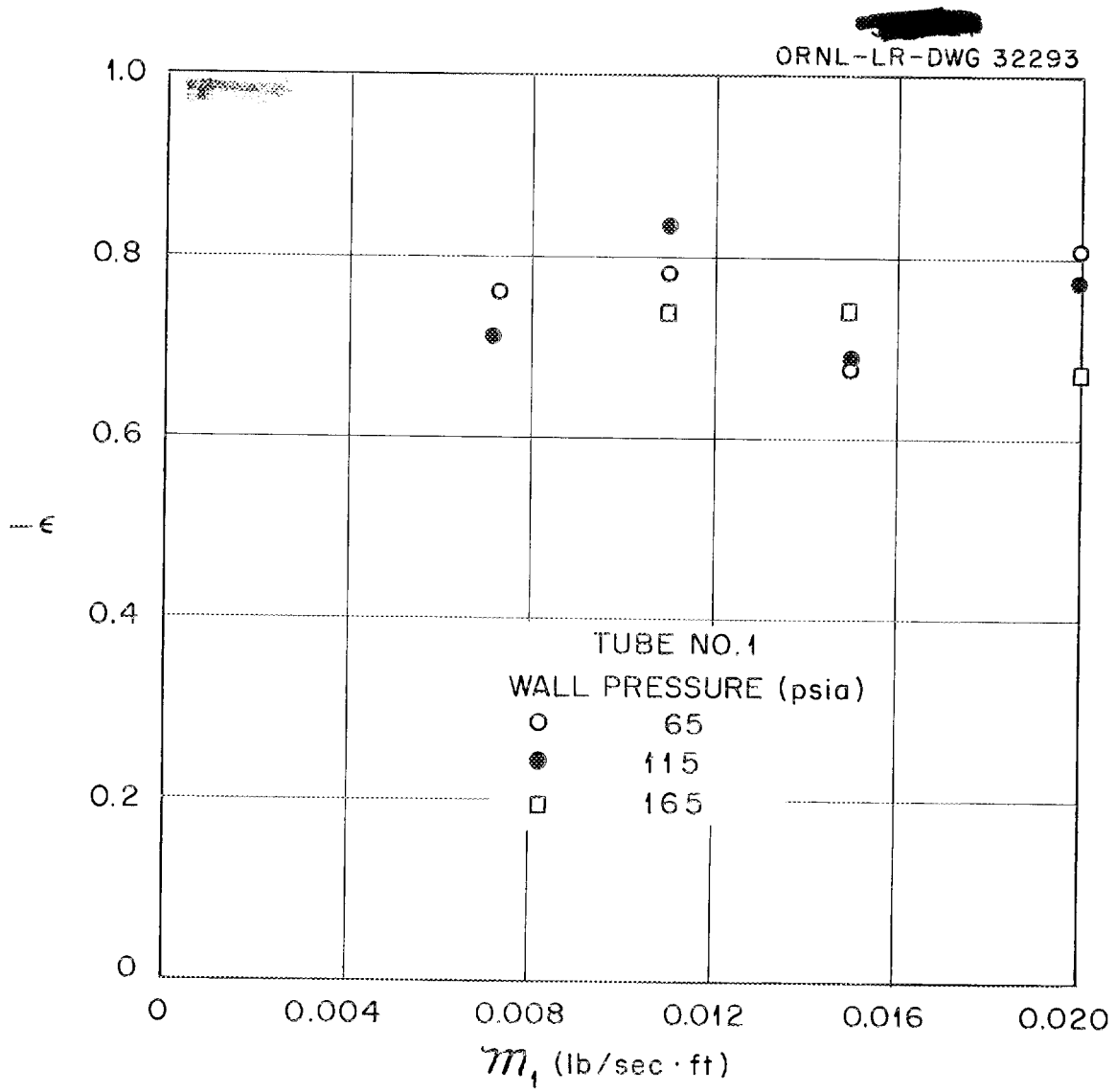

Fig. 9. Variation of ϵ in $\nu \propto r^{+\epsilon}$ with Mass Flow Rate per Unit of Tube Length, and Tube Pressure, for Tube No. 1.

be either a Reynolds number effect or an effect due to the change in jet exit Mach number with changing tube pressure.

The variation of the ratio of the actual tangential Mach number of the vortex to the ideal jet exit Mach number with $\mathcal{M}_1$ and tube pressure is shown in Fig. 10 for tube No. 2 and in Fig. 11 for tube No. 1. If the flow were inviscid, the ratio would, of course, be unity. It is much less than unity, as a result of the high viscous torque exerted on the fluid by the turbulent shear layer at the tube wall. It was predicted in Ref. 1 that for a laminar vortex the "effectiveness of vortex formation" M_p/M_j should increase as $\mathcal{M}_1$ increased, because the ratio of the torque exerted on the fluid in the tube, by the entering jet for a given value of M_p/M_j to the torque exerted by the wall shear layer, increases with $\mathcal{M}_1$. This effect is also present in the turbulent case, as may be seen most easily from Fig. 11. However, because the effective viscosity is increased by turbulence, a much higher mass flow rate would be required to approach the inviscid vortex with turbulent flow than with laminar flow. The mass flow rates required to generate turbulent vortices having tangential Mach numbers near unity would be an order of magnitude higher than can be tolerated by the diffusion process at that tangential Mach number. It is therefore concluded that some means of stabilizing the shear layer on the tube wall, or otherwise reducing the viscous retarding torque, is essential to the production of vortices of sufficient strength for the vortex reactor application.

[redacted]

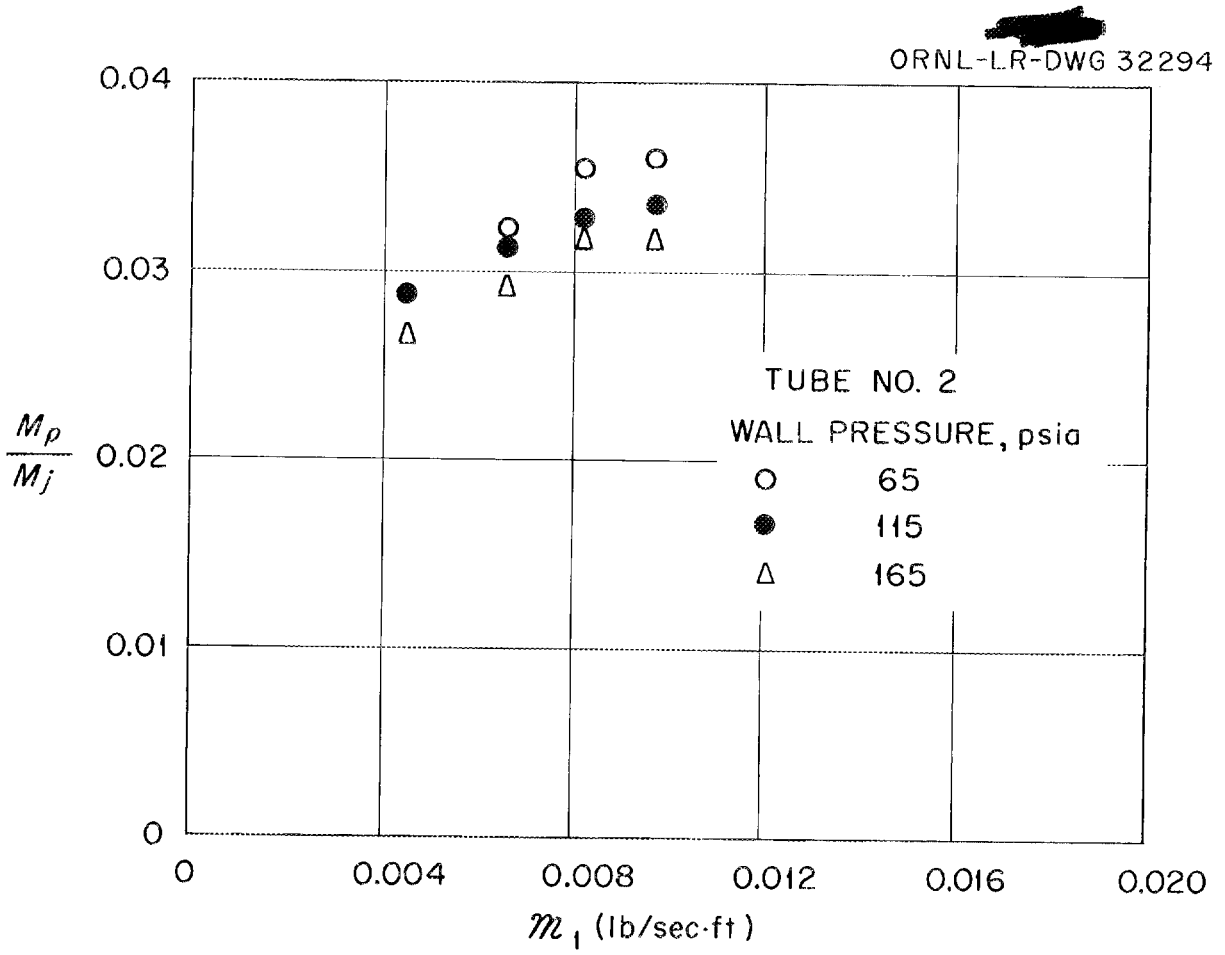

Fig. 10 Variation of Ratio of Vortex Tangential Mach Number and Jet Exit Mach Number With Mass Flow Rate per Unit of Tube Length, and Tube Pressure, for Tube No. 2.

[redacted]

[redacted]

ORNL-LR-DWG 32295

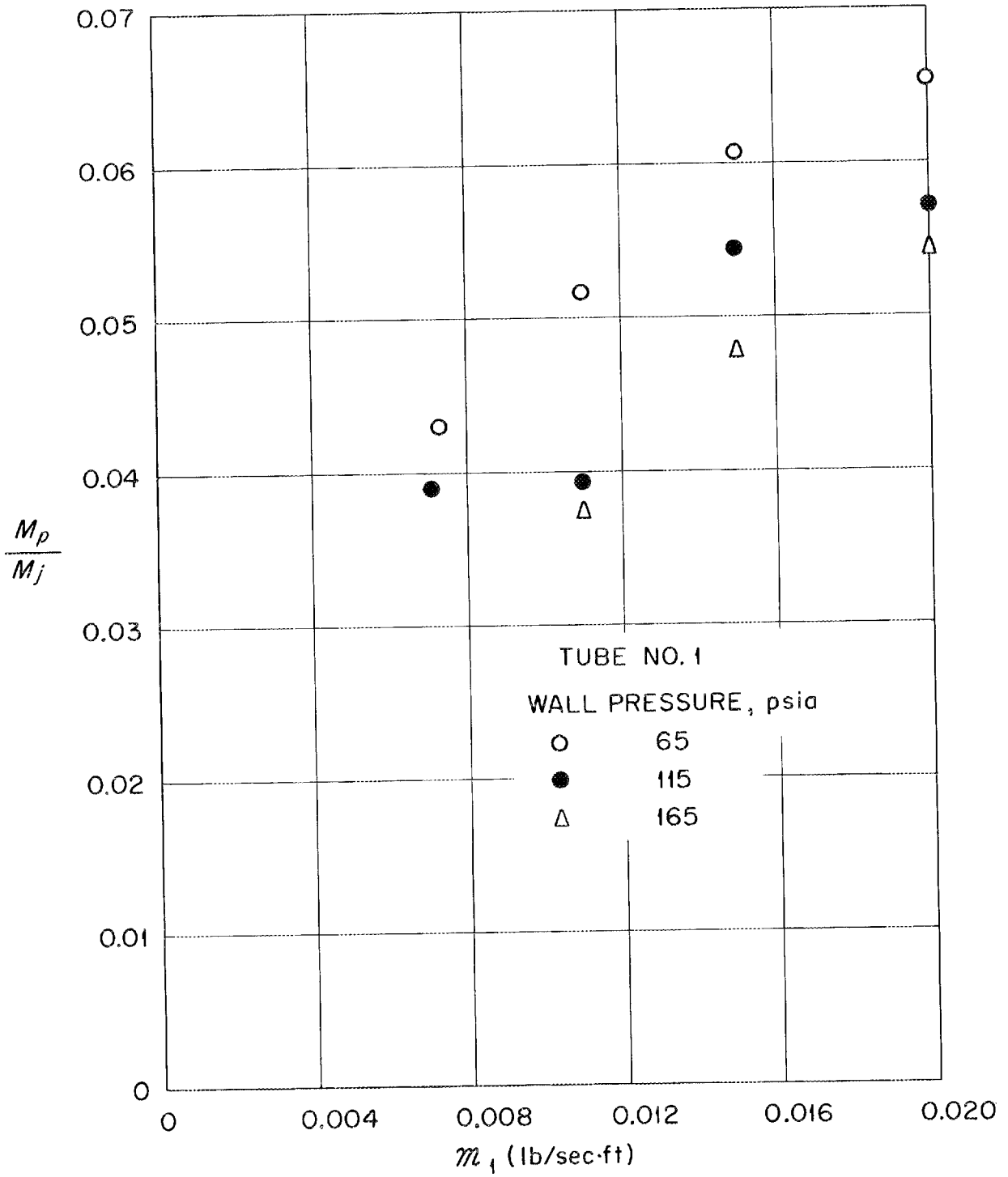

Fig. 11. Variation of Ratio of Vortex Tangential Mach Number and Jet Exit Mach Number With Mass Flow Rate per Unit of Tube Length, and Tube Pressure, for Tube No. 1.

Influence of Exit Nozzle on Vortex Structure

As the center of the vortex is approached, the radial velocity, u, must approach zero as the fluid turns and flows axially down through the tube and out the exit nozzle at one end. Thus as the center of the tube is approached, the differential equation governing the tangential velocity becomes that which is obtained by putting the right side of Eq. 1 equal to zero. The solution of this equation is the familiar "solid body rotation", for which v is proportional to r. On the other hand, it has been demonstrated that in the outer portion of the tube Eq. 1 describes the variation of the tangential velocity quite accurately if $\mu/\rho ur$ is taken as a constant slightly less than unity. The flow then approaches a free vortex, with v proportional to r^{ϵ} where $-\epsilon$ is near unity.

Between the free vortex region and the center, the flow therefore changes character as $\mu/\rho ur$ changes from a comparatively small value to a very large one. As a first approximation, it will be assumed that $-\rho ur$ varies linearly with r' between zero and some r'_t, which is characteristic of the exit nozzle radius, and that $-\rho ur$ is constant for r' greater than r'_t. Then for r' greater than r'_t, the tangential velocity is given by Eq. 3. For r' less than r'_t, Eq. 1 becomes

$$\frac{dv'}{dr'} + \frac{v'}{r'} = - \frac{K}{r'/r'_t} \quad r' \left\{ \frac{d^2v'}{dr'^2} + \frac{1}{r'} \frac{dv'}{dr'} - \frac{v'}{r'^2} \right\} \tag{7}$$

It is convenient to write the equation in terms of $r^* \equiv r'/_t$ and $v^* \equiv v'/v(r'_t)$. We then have

$$r^{*2} \frac{d^2v^*}{dr^{*2}} + r^* \left(1 + \frac{r}{K}\right) \frac{dv^*}{dr^*} - \left(1 - \frac{r^*}{K}\right) v^* = 0 \tag{8}$$

[redacted]

This equation has been integrated for several values of K. The results are plotted in Fig. 12.

If M_t is the tangential Mach number of the vortex at r'_t, then from Eq. 5 the pressure distribution is given by

$$\frac{1}{p^*} \frac{dp^*}{dr^*} = \gamma M_t^2 \frac{v^{*2}}{r^* T^*} \quad ;$$

and if $T^* = p^{*\frac{\gamma - 1}{\gamma}}$, we find upon integration,

$$\frac{1 - p^{*\frac{\gamma - 1}{\gamma}}}{(\gamma - 1) M_t^2} = \int_{r^*}^{1} \frac{v^{*2}}{r^*} dr^* \equiv I (r^*, K) \quad . \tag{9}$$

Values of I (0, K), computed from the values of Fig. 12, are given in Fig. 13.

From the previous analysis of the portions of the flow with ρur constant, K is known for a given experimental run, hence the integral is known as a function of r^*. But the left-hand side of Eq. 9 can also be computed from the experimental data, and is a function of both r^* and r'_t. If a given value of r^* is selected, then r'_t may be dtermined from Eq. 9. The radius r'_t has been determined in this way, for $r^* = 0$, for runs made with two different exit nozzle configurations. In the first run, the nozzle was an annulus, with 0.28-in. outside diameter. In the second run, the nozzle was a central hole 0.125 in. in diameter. The experimental pressure distributions for these two runs are shown in Fig. 14, with the values of K and ϵ determined by the procedure outlined in the preceding section. The values of r'_t, M_t, and I (0, K) found by the procedure outlined above are also given.

[redacted]

ORNL-LR-DWG 32296

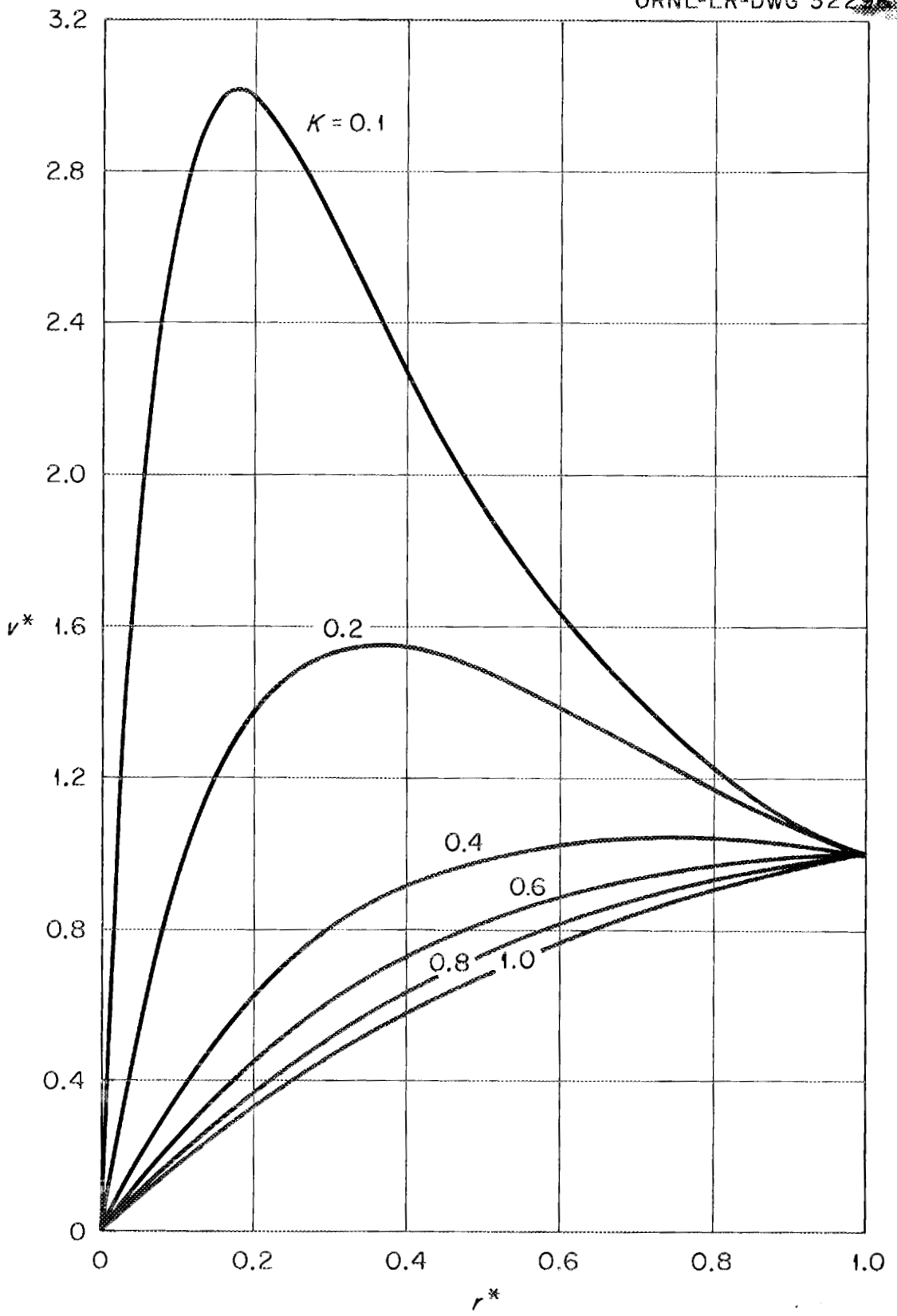

Fig. 12. Variation of Tangential Velocity With Radius Within Region Influenced by Exit Nozzle Outflow, for Various Effective Viscosities, K.

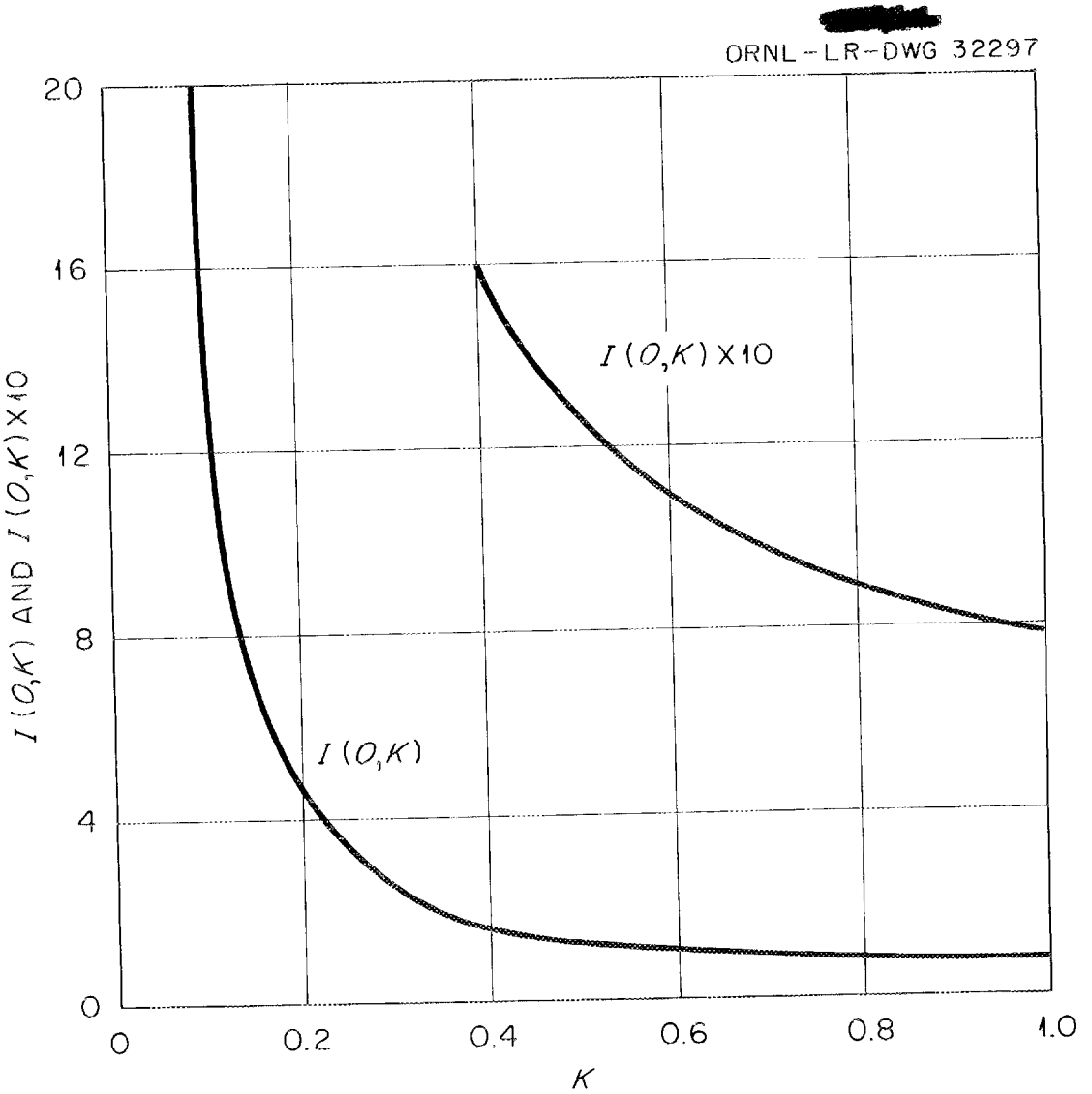

Fig. 13. Dependence of $I(O,K)$ on the Effective Viscosity, K.

[redacted]

ORNL-LR-DWG 32298

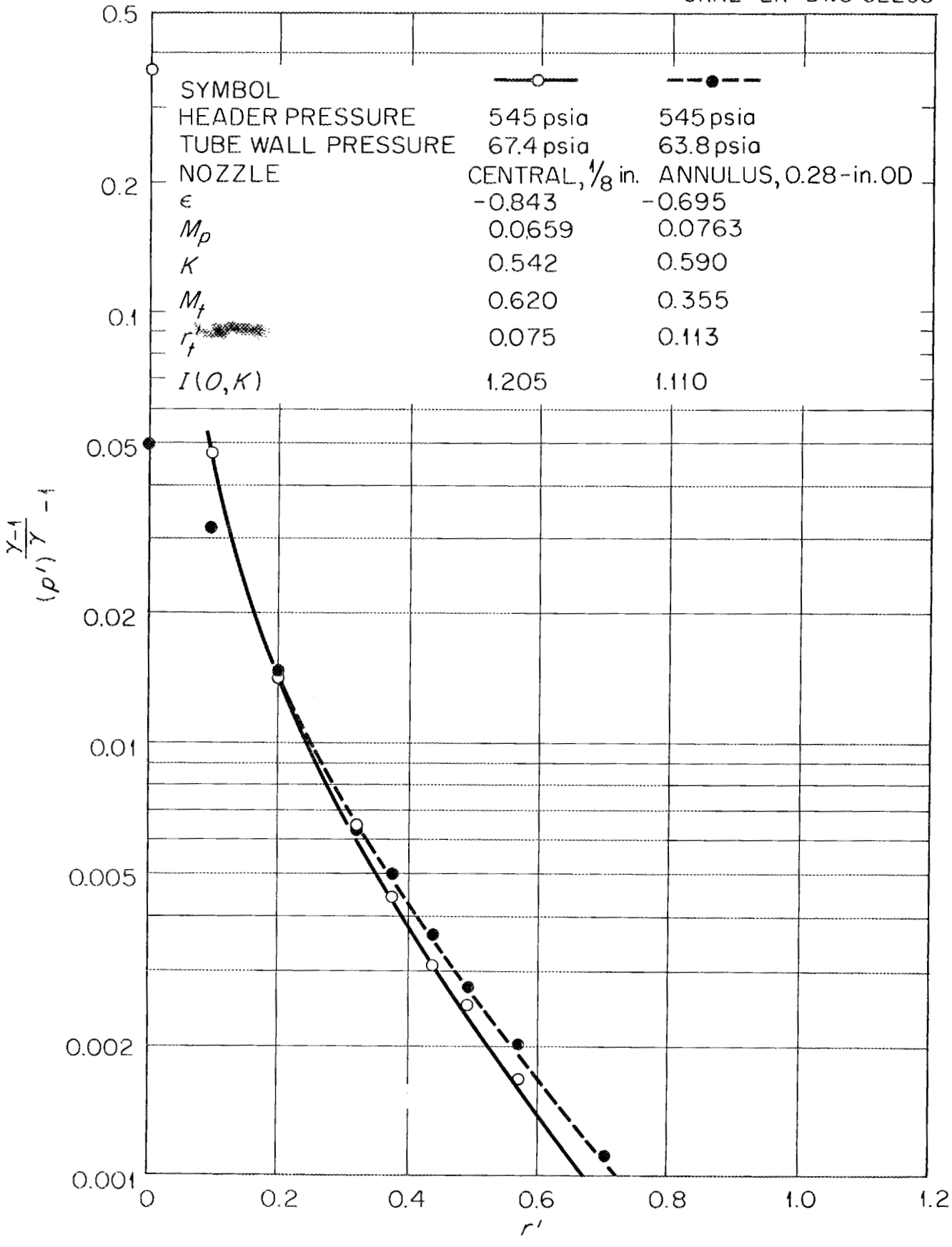

Fig. 14. Pressure Distributions and Correlation Parameters for two Different Exit Nozzle Configurations.

The values of r'_t do not agree exactly with the value of r' corresponding to the nozzle radius, being 20 per cent smaller for the annular nozzle and 20 per cent larger for the central nozzle. This spread can probably be attributed to the different nozzle geometry, i.e., to the blockage at the center of the annulus nozzle. In any case, two conclusions seem justified. First, the effect of the outlet flow on the vortex structure can be approximated by the model given here, with r'_t close to the value of r' corresponding to the nozzle radius. Second, the values of K, deduced previously from the exponent in $v \propto 1/r^{\epsilon}$, are of the right order of magnitude to explain also the behavior of v near the nozzle radius. These are really two independent checks on K, so that the values presented in Fig. 14 can be given with some confidence.

On the basis of this analysis, it is therefore felt that if the effective viscosity is known for the body of the vortex, the influence of the outflow through the nozzle on the vortex strength near the center can be predicted, at least approximately, by the method given.

Preliminary Separation Experiments

The tangential Mach number of the vortices generated in the above experiments increases very rapidly with the decreasing radius, because of the decrease in temperature with decreasing radius, as well as the increase in the tangential velocity. Therefore, although the tangential Mach numbers near the outside of the tube are much too small to allow a concentration of heavy gas near the wall of the tube, there is a possibility of obtaining a concentration very near the center of the tube, if a sufficiently small exit nozzle is used.

This possibility has been explored with helium as the light gas, and both bromine and a heavy fluorocarbon (C_8F_{16}) as heavy gases.

Bromine Separation

Bromine vapor, which at room temperature is reddish brown and readily observed by eye, was used as a heavy gas with helium. A light source was focused on the exit plate of the vortex tube through a ground-glass diffuser plate, to produce uniform illumination across the tube.

Figs. 15 (left) and 15 (right) are black and white prints of Ektachrome pictures taken axially along the tube under the operating conditions summarized in the first two lines of Table I. It is believed that the small dark annulus near the center of the tube in the left photograph is a gaseous concentration of bromine while the larger dark ring is a cloud of condensed bromine.

It is difficult to avoid the condensation, because the concentration of bromine which is required for visibility is near the saturation concentration at the conditions existing in the tube. For comparison, a case in which no such gaseous separation can be detected in the photograph, but in which a cloud was formed, is shown at the right of Fig. 15.

The pressure distributions for the above two cases are shown in Fig. 16, the upper curve corresponding to the photograph at the left in Fig. 15, and the lower curve to the photograph at the right. Both the experimental points and the fitted curves from Eq. 6 are shown. From the values of ϵ and M_p obtained by fitting the pressure distributions, the variation of the tangential Mach number with tube radius can be computed. The Mach numbers are shown in Fig. 17.

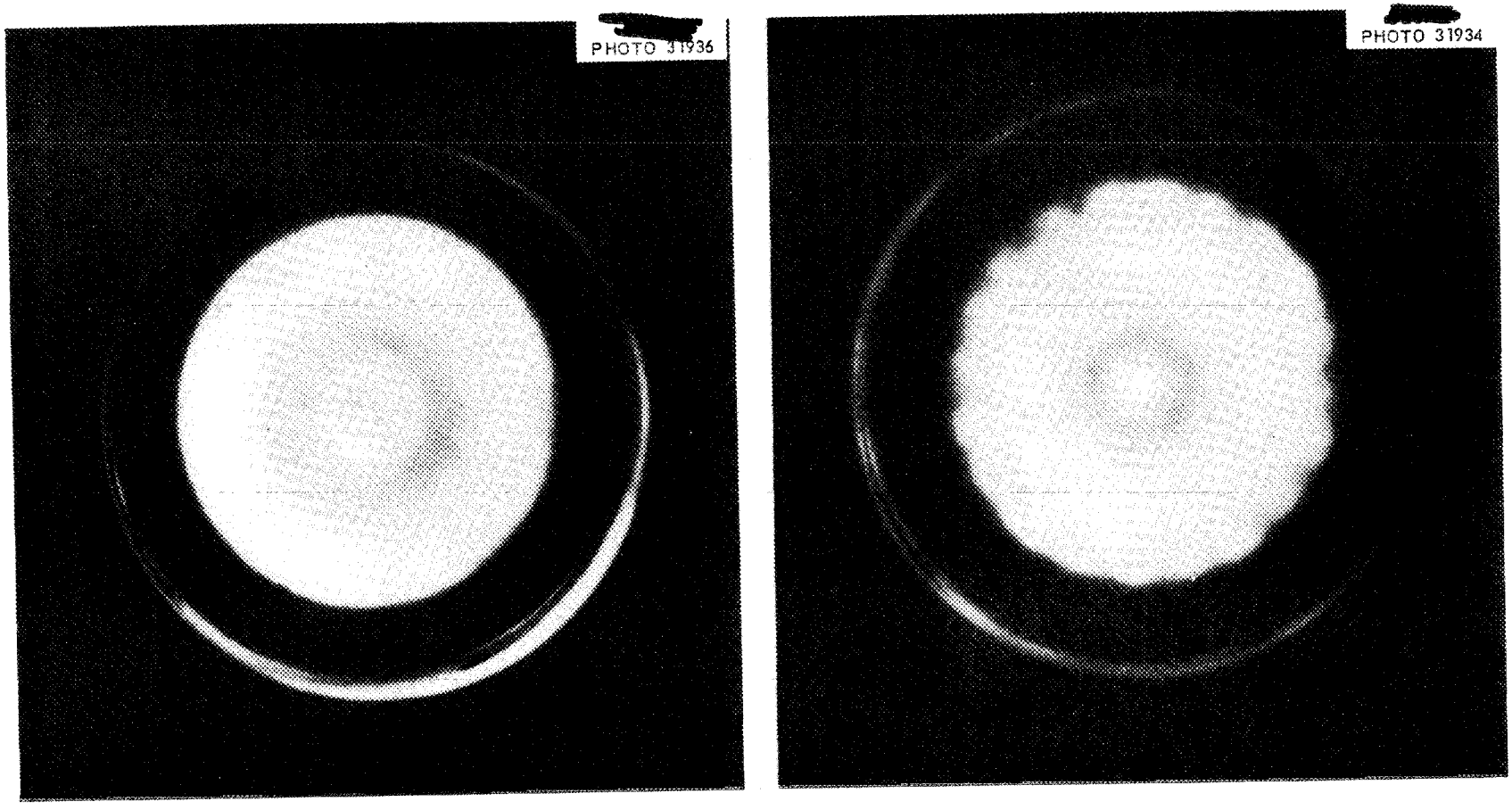

Fig. 15. Photographs Taken Axially Through Vortex Tube Operating With He and Br_2, Showing at The Left a Large Ring of Condensed Br_2, and at The Right Only The Condensed Br_2.

TABLE I. SUMMARY OF OPERATING CONDITIONS FOR THE SEPARATION EXPERIMENTS

Fig. No.	Vortex Tube	Exit Plate Configuration	Heavy Gas Feed	Header Pressure psig	Tube Wall Pressure psig	Gas Pair	Mass Flow lb/sec	Temp. of Feed Gas °F
18 (left)	1	3/16-in.-dia hole	Radial thru probe tap 3 in. from static end	400	49	He-Br_2	0.0055	80
18 (right)	1	3/32-in.-dia center hole, 20 - 0.028-in.-dia peripheral holes	Radial thru probe tap 3 in. from static end	400	38	He-Br_2	0.00183 radial, 0.00412 periph.	80
21, A	2	3/16-in. center hole	Tangential thru four headers (12 nozzles)	625	37	He-C_8F_{16}	0.00410	79
21, B	2	3/16-in. center hole	Axial thru end pressure taps at $r' = 0.093, 0.20, 0.32, 0.375$	625	36	He-C_8F_{16}	0.00410	77

[redacted]

ORNL-LR-DWG 32299

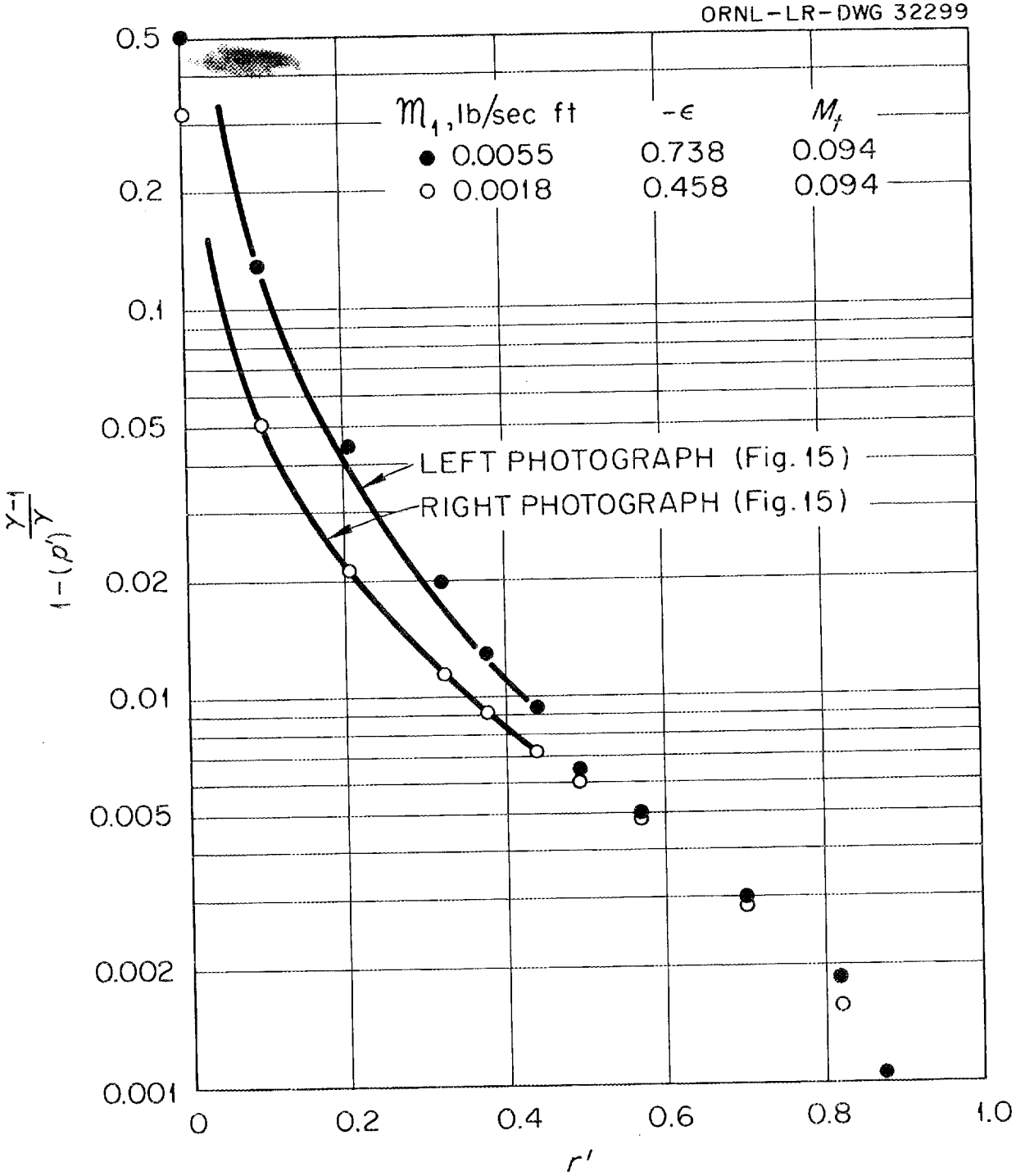

Fig. 16. Pressure Distributions Corresponding to the Photographs of Fig. 15.

[redacted]

ORNL-LR-DWG 32300

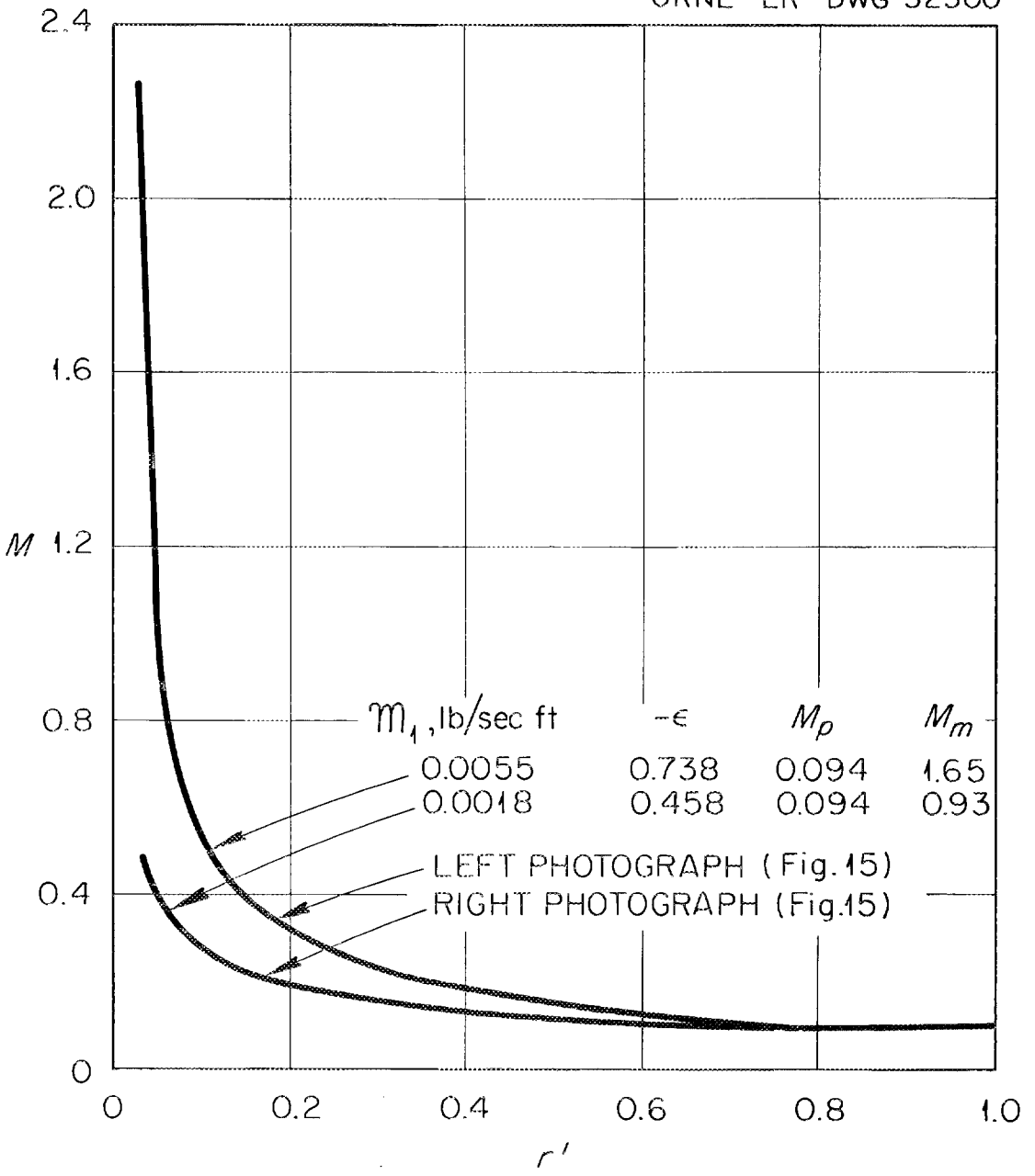

Fig. 17. Mach Number Distributions Corresponding to the Photographs of Fig. 15, with Values of Mach Number Required for Separation, M_m.

It was found in Ref. 1 that, at the tube radius where the maximum ratio of heavy and light gas densities occurs, a simple relation exists between the tangential Mach number, the radial mass flow rate, the fluid density, and the binary diffusion coefficient. If the heavy gas density and mass flow rate are small compared to the light gas density and mass flow rate, the relation is,

$$\frac{2\pi\rho_m D_{12}}{\mathcal{M}_1} = \frac{1}{\gamma M_m^{\,2}\left(\frac{\mathcal{M}_2}{\mathcal{M}_1} - 1\right)} \tag{7}$$

where

ρ_m ≡ gas density at radius of maximum density ratio

D_{12} ≡ binary diffusion coefficient at same point

$\mathcal{M}_1$ ≡ radial mass flow per unit of tube length

γ ≡ ratio of specific heats for light gas

M_m ≡ tangential Mach number at radius of maximum density ratio

$\mathcal{M}_2/\mathcal{M}_1$ ≡ ratio of masses of heavy and light gas molecules

The diffusion coefficient was computed by methods of Ref. 4 for helium and bromine.

Values of M_m are listed on Fig. 17. Comparison of the computed value of $M_m = 1.65$ for the upper curve, with the values of M computed from the pressure distribution, indicates that for this case a concentration peak would indeed be expected for a radius of about 0.03 in. This agrees with the size of what appears to be a clear core in the photograph at the left of Fig. 15. Conversely, from the lower curve of Fig. 17 and the value of $M_m = 0.93$, it seems unlikely that a high enough Mach number for separation

was attained in the case shown at the right of Fig. 15, and no separation could be detected in this case.

The agreement between theory and experiment is really somewhat better than might be expected, in view of the fact that the flow in the tube is turbulent, while the calculation of Ref. 1 assumed laminar flow. It is possible, however, that the pressure drop experienced by the gas as it flows inward is sufficient to reduce the turbulent fluctuations near the center of the vortex to a very low intensity.

Fluorocarbon Separation

The heavy fluorocarbon (C_8F_{16}*) is stable, relatively inert, and has sufficient volatility (35 mm Hg) at room temperature to permit significant gas phase concentrations. These properties, together with its molecular weight of 400, make it an almost ideal heavy gas for separation experiments. However, it cannot be detected visually, and its diffusion properties with helium are not known.

In the experiments to be described here, a very fine radial probe was used to sample the gas mixture in the vortex tube. Fig. 18 is a sketch of the probe showing the geometry of the telescoping segments, the smallest of which is 0.008-in. outside diameter with a 0.004-in. opening. The largest tube in contact with the vortex field near the wall is 0.017-in. outside diameter. Even this relatively small probe has a measurable effect on the vortex strength as shown in Fig. 19, in which the pressure ratios are those measured at the closed end; the probe was positioned 3 in. from the exit plate. Of course, it is possible that the disturbance created at the tip

*Perfluorodimethylcyclohexane

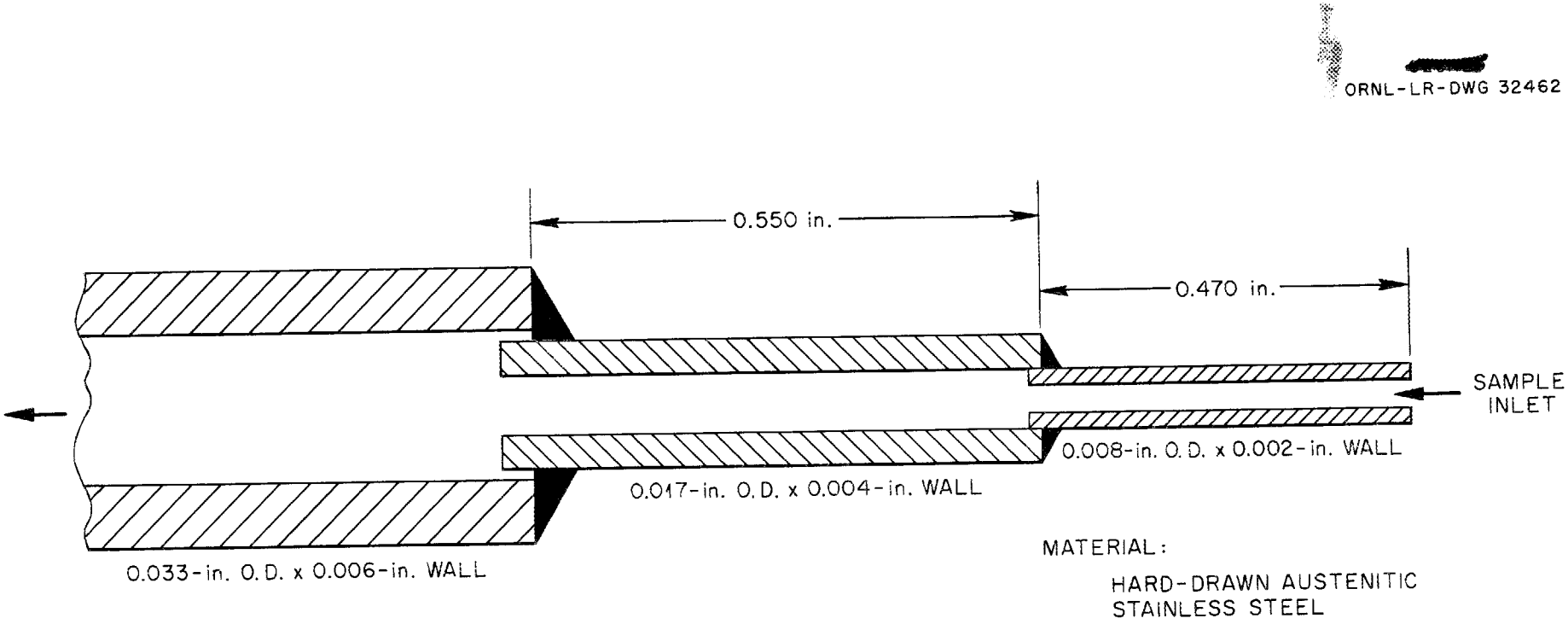

Fig. 18. Sample Probe Detail.

[redacted]

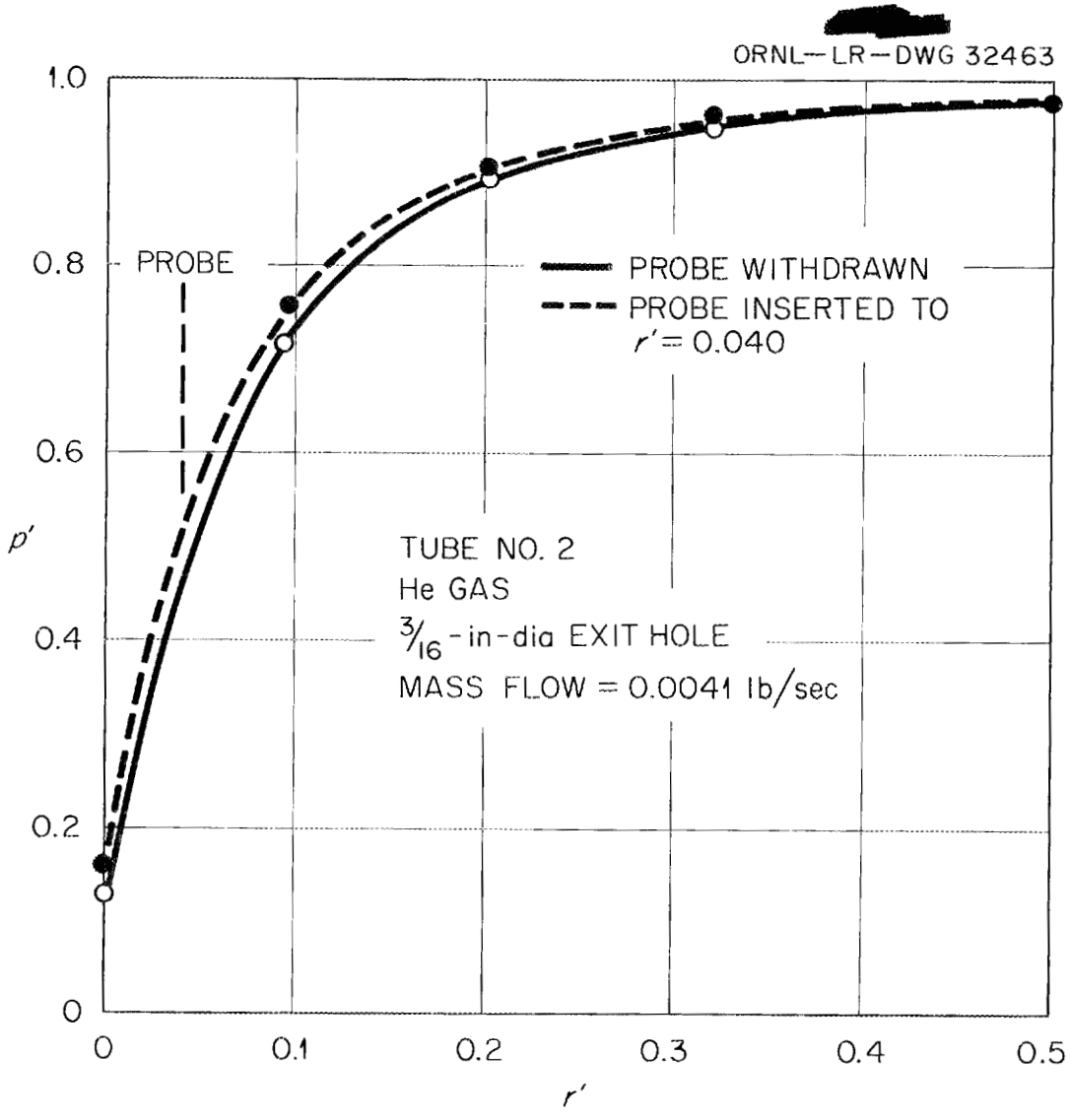

Fig. 19. Effect of Sampling Probe on Pressure Distribution.

of the probe may have an effect much greater than that indicated in the figure. In fact, there is some evidence that the vortex center is displaced inwardly and that the probe is deflected slightly by the circulating gas so as not to intersect the true centerline of the tube. It seems reasonable to believe that the influence of the probe will fall off rapidly for positions beyond $r' = 0.050$ and the concentration data to be presented should be interpreted with this in mind.

The sample was led to a thermal conductivity cell. The instrument, a GOW-Mac Instrument Company Model NRL small volume, four filament cell, was connected as shown in Fig. 20. The cell was balanced to give zero output with pure helium on the reference and sample sides simultaneously. The sample was then admitted and the output read on a sensitive potentiometer. Note that the cell was operated at 10 cm Hg absolute in order to decrease response time for the small sample flows of about 25 standard cc per minute. The calibration is linear, with a slope of 10.2 mv/per cent C_8F_{16} at a total cell current of 150 ma.

Measured mole-fraction distributions of C_8F_{16} are shown in Fig. 21 for two methods of introduction of the heavy gas. The tests were conducted in tube No. 2 with the operating conditions given in the last two lines of Table I. In the test corresponding to curve A, the fluorocarbon was introduced through the tangential nozzles with the helium. In the test corresponding to curve B, the fluorocarbon was introduced through pressure taps in the closed end of the vortex tube. The manner of introduction of the heavy gas has a pronounced effect on the concentration profile near the outside of the tube, because the separation effect in this case is so weak

[redacted]

ORNL-LR-DWG 32461

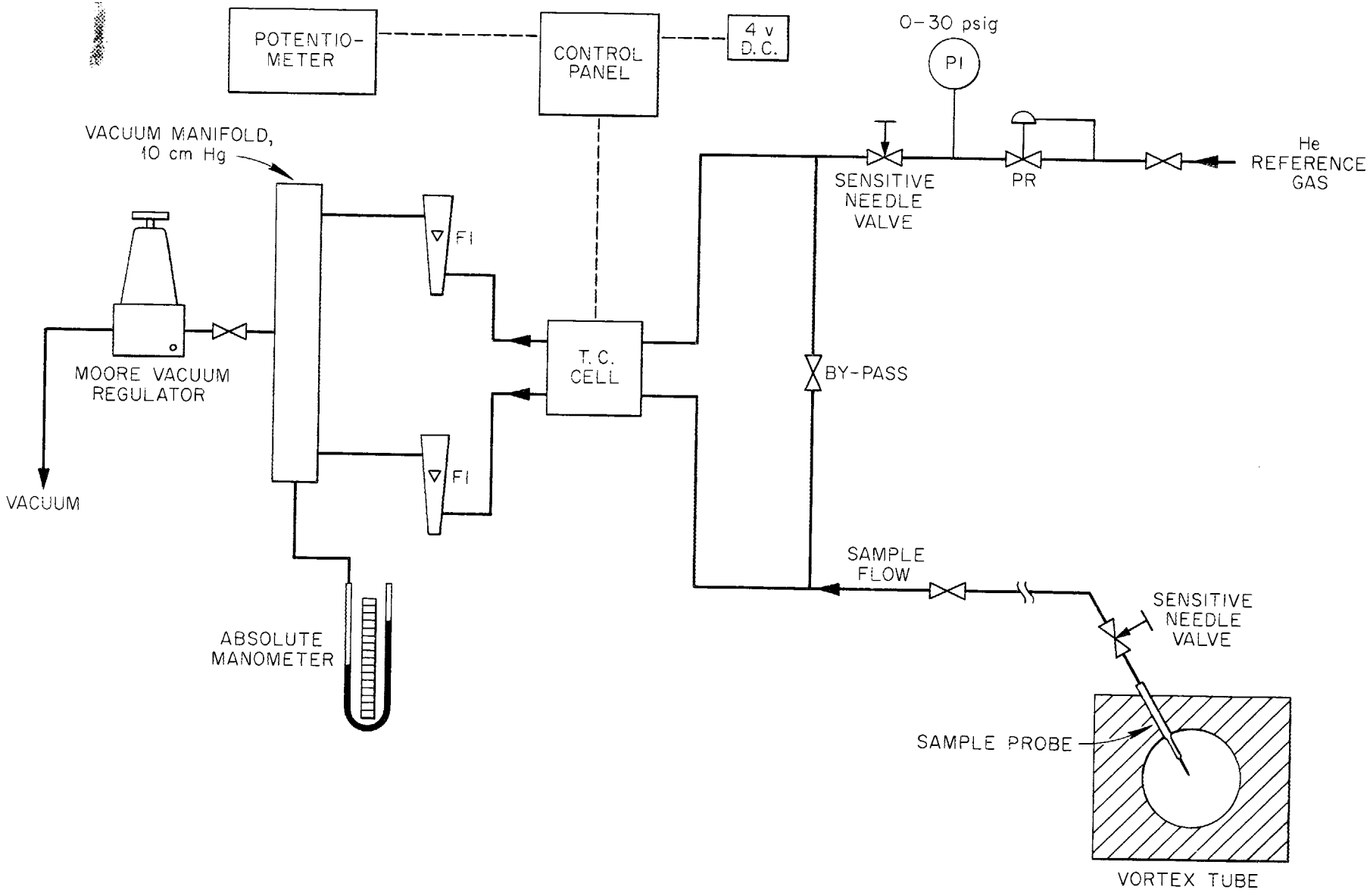

Fig. 20. Gas Analysis Apparatus.

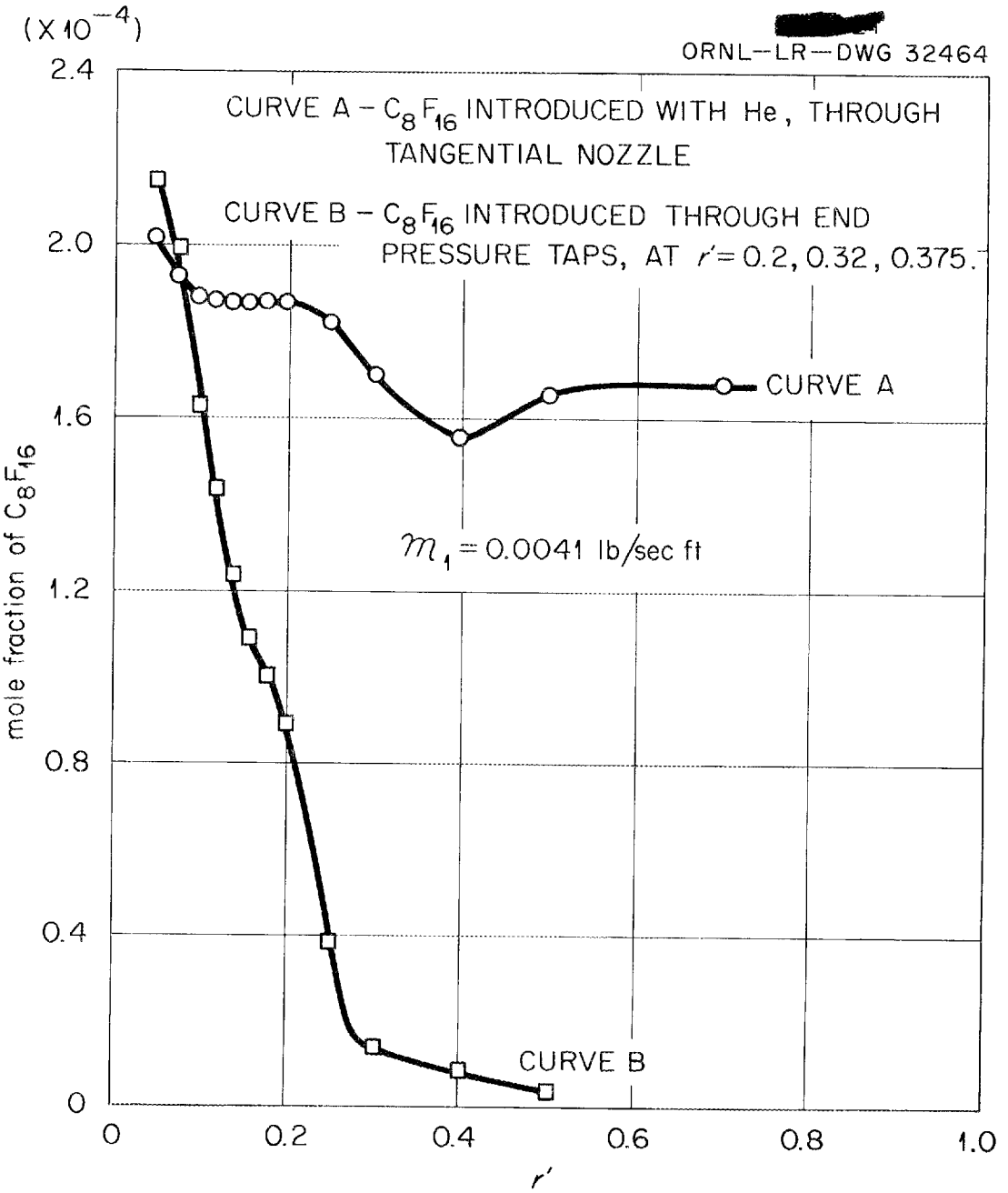

Fig. 21. Measured mole Fraction of C_8F_{16} in Helium, for two Modes of Introduction of the Fluorocarbon.

that the residence time of the heavy gas in the tube is not large compared to that of the light gas.

In both of the cases shown, a sharp rise in the mole fractions exists up to about $r' = 0.05$. If it had been possible to continue the measurement to $r' = 0$, it is expected that the mole fraction would have decreased again. This was not possible for the two reasons given above: that the probe was deflected by the flow, and that it may have disturbed the flow near the core of the vortex.

The inflections in both curves A and B at about $r' = 0.15$ are probably due to a cloud of droplets similar to that seen in the photograph of the bromine-helium tests. Since the response of the probe to these droplets was not known, no quantitative information about the cloud other than its position can be gained from the measurement.

It is believed that, although these data are somewhat uncertain, they indicate that a peak in mole fraction of gaseous C_8F_{16} probably existed in both cases, and that the position of this peak was inside of $r' = 0.05$. A calculation of the radius at which the peak would be expected has been carried out, as for the bromine-helium core. The diffusion coefficient for helium and C_8F_{16} is not known, but a value was estimated from data on cyclohexane. The pressure and Mach number profiles are shown in Figs. 22 and 23, with the estimated value of $M_m = 1.1$. This gives the expected position of the mole-fraction peak as about $r' = 0.04$, which is quite consistent with the data of Fig. 21.

Thus, it is felt that the data for helium and C_8F_{16} substantiate the conclusions reached for helium and bromine.

[redacted]

ORNL-LR-DWG 32465

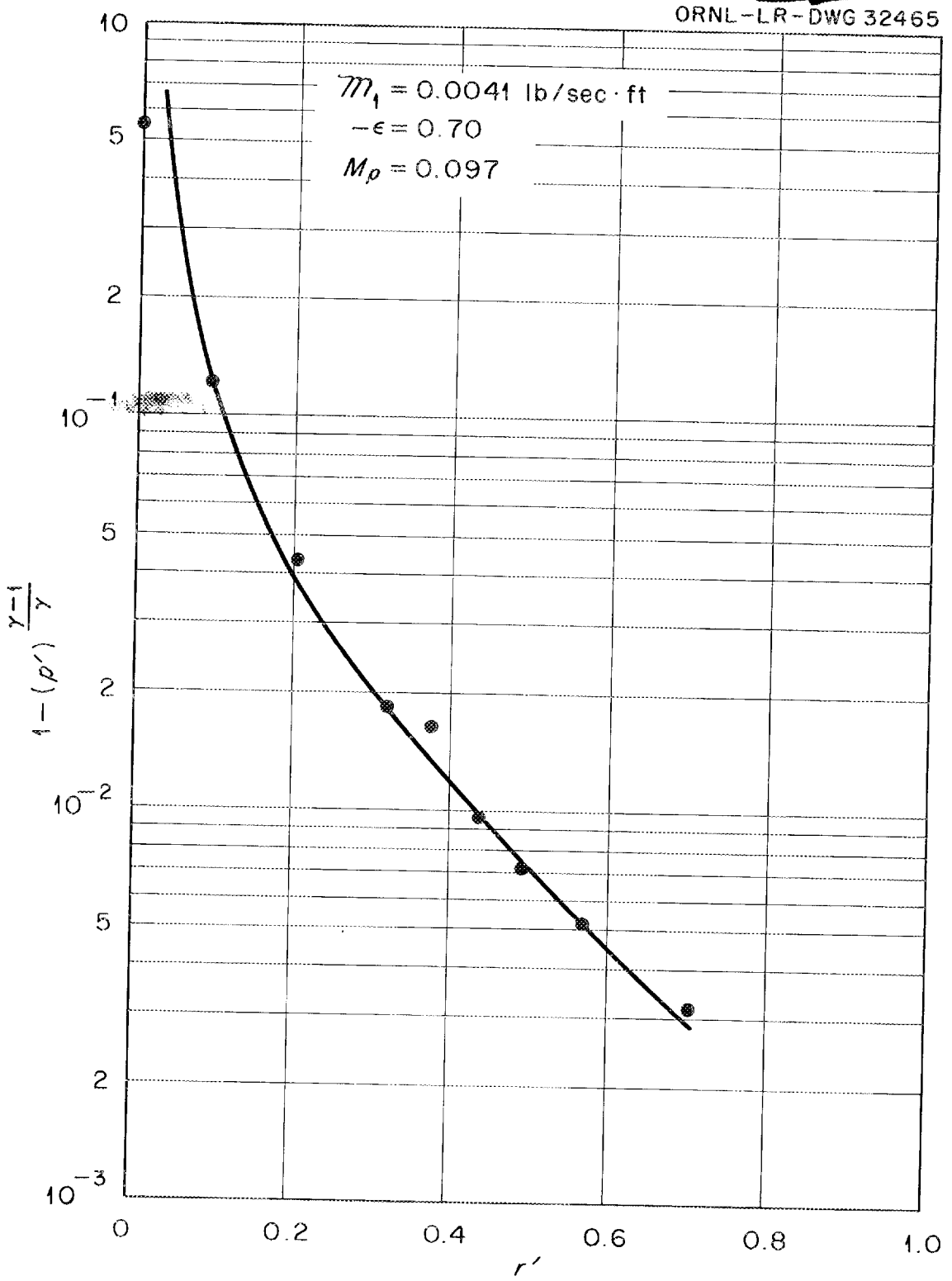

Fig. 22. Pressure Profile Corresponding to Fig. 21.

[redacted]

[redacted]

ORNL-LR-DWG 32466

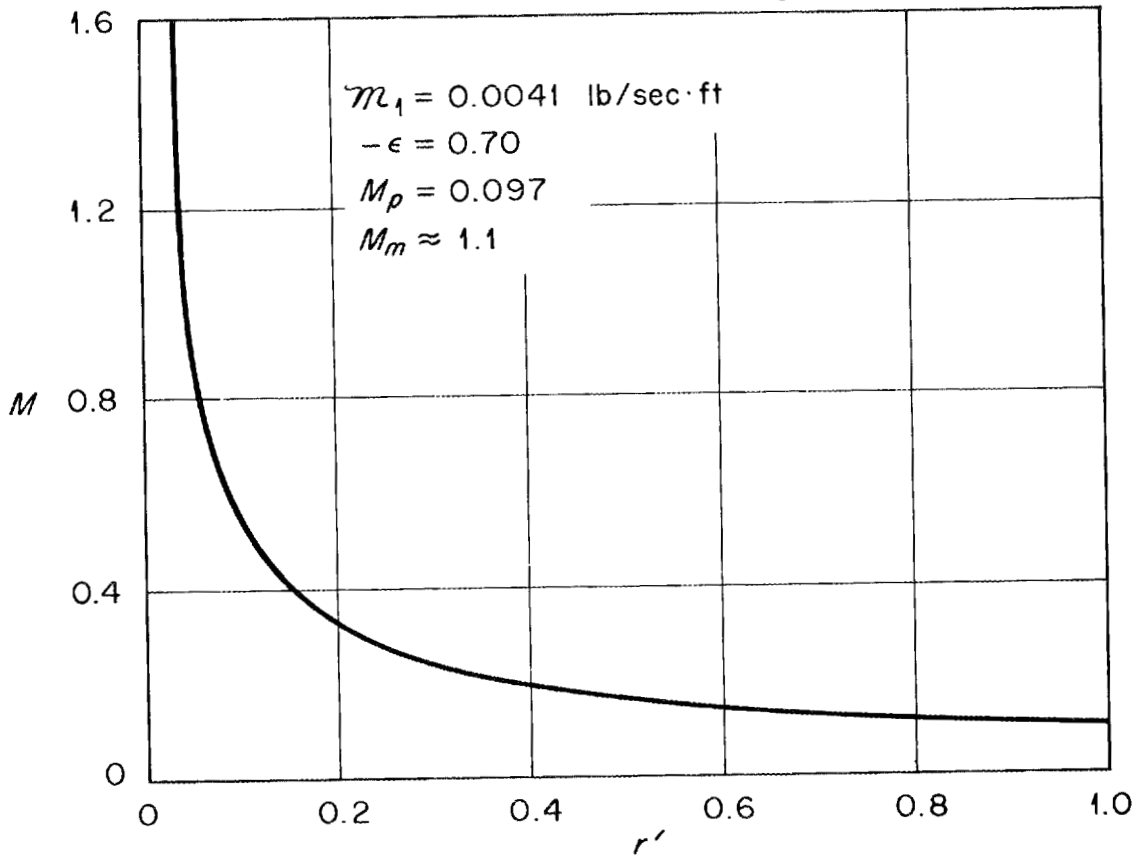

Fig. 23. Mach Number Profile Corresponding to Fig. 21.

CONCLUSIONS

On the basis of the preceding data and analysis, the following conclusions seem justified:

1. In a simple vortex tube such as that sketched in Fig. 1, the flow is turbulent at mass flow rates of interest, and the viscous effects are so strong as to prevent formation of vortices of adequate strength for application to vortex reactors. It is therefore concluded that some means of stabilizing the shear layer on the tube wall, or otherwise reducing the viscous retarding torque, is essential to the production of vortices of sufficient strength for the vortex reactor application.

2. Even though the viscous effects are strong, the variation of tangential velocity with radius may approximate that of an inviscid vortex.

3. A simple model has been developed which predicts, at least approximately, the influence of nozzle outflow on the vortex structure near the center of the tube.

4. It is believed that preliminary separations of helium from both bromine and a heavy fluorocarbon have been obtained, although the interpretation of the experimental data is somewhat difficult. The tube operating conditions under which separation was achieved are not suitable for application to a vortex reactor. Reasonably good agreement between the positions of the heavy gas mole-fraction peaks and the positions predicted by the analysis of Ref. 1 were found.

REFERENCES

1. Kerrebrock, J. L., and R. V. Meghreblian, An Analysis of Vortex Tubes for Combined Gas-Phase Fission Heating and Separation of the Fissionable Material, ORNL-CF 57-11-3, Rev. 1, April 11, 1958.

2. Hartnett, J. P., and E. R. Eckert, Experimental Study of the Velocity and Temperature Distributions in a High Velocity Vortex Type Flow, Heat Transfer and Fluid Mechanics Institute, Stanford University Press, 1956.

3. Kerrebrock, J. L., and P. G. Lafyatis, Analytical Study of Some Aspects of Vortex Tubes for Gas-Phase Fission Heating, ORNL-CF 58-7-4, July 21, 1958.

4. Rossini, F. D., Thermodynamics and Physics of Matter, Princeton University Press, 1955.

INTERNAL DISTRIBUTION

1. F. F. Blankenship
2. E. P. Blizard
3. R. A. Charpie
4. W. K. Ergen
5. A. P. Fraas
6. J. H. Frye, Jr.
7. B. L. Greenstreet
8. W. R. Grimes
9. H. W. Hoffman
10. J. J. Keyes, Jr.
11. W. D. Manly
12. A. J. Miller
13. R. F. Newton
14. J. A. Swartout
15. A. M. Weinberg
16. E. P. Wigner
17. M. J. Skinner
18-32. Laboratory Records Department
33. Laboratory Records, ORNL R.C.

EXTERNAL DISTRIBUTION

34-37. Air Force Ballistic Missile Division
38. AFPR, Douglas, Long Beach
39. AFPR, North American, Canoga Park
40. AFPR, North American, Downey
41-42. Air Force Special Weapons Center
43. Air Research and Development Command (RDTAPS)
44. Air Research and Development Command (RDZN)
45. Air Technical Intelligence Center
46. ANP Project Office, Convair, Fort Worth
47. Albuquerque Operations Office
48. Argonne National Laboratory
49. Armed Forces Special Weapons Project, Sandia
50. Armed Forces Special Weapons Project, Washington
51-52. Army Ballistic Missile Agency
53. Army Rocket and Guided Missile Agency
54. Assistant Secretary of Defense, R&D (WSEG)
55-58. Atomic Energy Commission, Washington
59. Atomics International
60. Brookhaven National Laboratory
61. Bureau of Aeronautics
62. BAR, Aerojet-General, Azusa
63. BAR, Chance Vought, Dallas
64-65. BAR, Martin, Baltimore (1 copy to C. D. Pengelley)
66. Bureau of Ordnance
67-68. Bureau of Ordnance (AD-1B)
69. Bureau of Ships
70. duPont Company, Aiken
71. General Electric Company (ANPD)
72-73. General Electric Company, Richland

74-78. Jet Propulsion Laboratory (1 copy ea. to F. Goddard, R. V. Meghreblian, H. J. Stewart, and P. Wegener)
79. Lockland Aircraft Reactors Operations Office
80-82. Los Alamos Scientific Laboratory (1 copy to J. Todd)
83. Marquardt Aircraft Company
84-85. National Advisory Committee for Aeronautics, Cleveland (1 copy to F. E. Rom)
86. National Advisory Committee for Aeronautics, Washington
87. New York Operations Office
88. Oak Ridge Operations Office
89. Office of Naval Research
90. Office of the Assistant for Operations Analysis DCS/O
91. Office of the Chief of Naval Operations
92. Office of the Chief of Ordnance, DOFL
93. Patent Branch, Washington
94. Phillips Petroleum Company (NRTS)
95. Pratt and Whitney Aircraft Division
96. San Francisco Operations Office
97-98. USAF Project Rand
99. U. S. Naval Ordnance Test Station
100-101. University of California Radiation Laboratory, Livermore
102-112. Wright Air Development Center
113-147. Technical Information Service Extension
148. Division of Research and Development, AEC, ORO